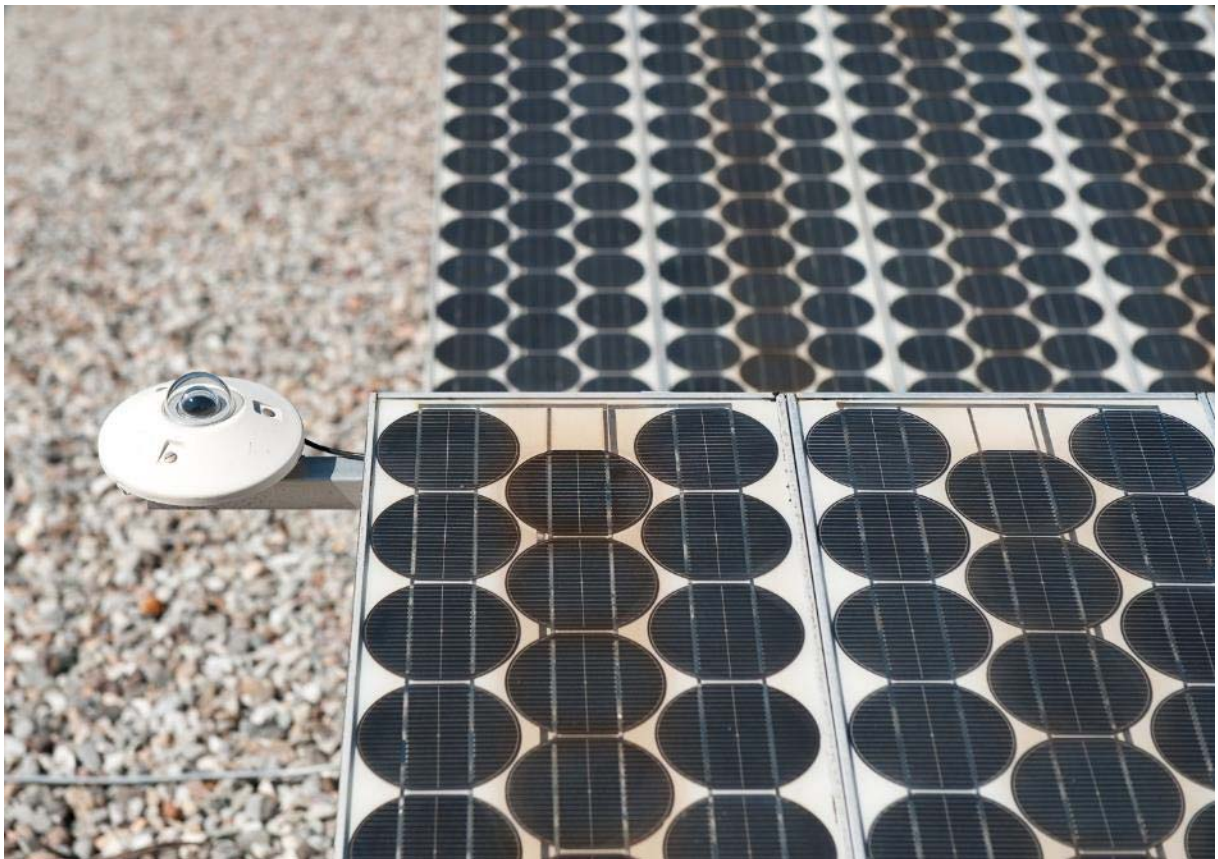




Final report

TISO 35+

Thirty-five years with the TISO-10 PV plant: a statistical analysis of failure modes and their impact on safety and production





University of Applied Sciences and Arts
of Southern Switzerland

SUPSI

Date: 19th November 2018

Place: Canobbio

Publisher:

Swiss Federal Office of Energy SFOE
Research Programme Photovoltaics
CH-3003 Bern
www.bfe.admin.ch
energieforschung@bfe.admin.ch

Agent:

SUPSI
Campus Trevano,
CH-6952 Canobbio
www.supsi.ch

EPFL STI IMT PV-LAB
MC A2 304 (Microcity)
Rue de la Maladière 71b
CH-2002 Neuchâtel 2
www.epfl.ch

Authors:

Mauro Caccivio, SUPSI, mauro.caccivio@supsi.ch
Alessandro Virtuani, EPFL, alessandro.virtuani@epfl.ch
Eleonora Annigoni, EPFL, eleonora.annigoni@epfl.ch

SFOE head of domain: Stefan Oberholzer, stefan.oberholzer@bfe.admin.ch
SFOE programme manager: Stefan Nowak, stefan.nowak@netenergy.ch
SFOE contract number: SI/501577-01

The author of this report bears the entire responsibility for the content and for the conclusions drawn therefrom.



Summary

The TISO-10 (Ticino SOLare) solar photovoltaic (PV) plant, connected to the grid in 1982, is the oldest installation of this kind in Europe. Besides its age, what makes the TISO-10 PV plant almost a unique-of-its-kind, is the fact that a set of 18 reference modules has been measured in laboratory at regular intervals and that these measurements are traceable to the original ones performed before installation. This makes prospectively the data that can be obtained from the TISO-10 PV system an extremely valuable data set of high-quality, which can be used to extrapolate with a larger accuracy long-term degradation curves and rates of the PV modules constituting the system. After 35 years, two different groups of PV modules can be identified; one with a negligible degradation rate of $-0.2\%/year$, the other with a degradation rate of $-0.69\%/year$, much higher but still compatible with a 25 years' warranty at 80% of the original power. Though there are multiple mechanisms, working together towards a faster, not linear degradation, the 21.5% of the PV modules is still in optimal shape and can be reinstalled targeting the next milestone: 40 years of operation. A comparative analysis of past and present technologies and of what can be learnt from yesterday's devices will complement this work.

Zusammenfassung

Die Solar-Photovoltaik-Anlage TISO-10 (Ticino SOLare), im Jahr 1982 an das Stromnetz angeschlossen, ist die älteste Anlage dieser Art in Europa. Was das TISO-10 neben seinem Alter einzigartig macht, ist die Tatsache, dass ein Satz von 18 Referenzmodulen im Laufe der Jahre regelmäßig im Labor getestet wurde und dass diese Messungen auf die ursprüngliche Messung von 1982 zurückzuführen sind. Dies macht prospektiv die Daten, die von der TISO-10-PV-Anlage erhalten werden können, zu einem äußerst wertvollen Datensatz von hoher Qualität, der verwendet werden kann, um langfristige Degradationskurven und -raten der PV-Module, die zur Anlage gehören, mit höherer Genauigkeit zu extrapolieren. Es können zwei verschiedene Gruppen von PV-Modulen identifiziert werden. Eine mit einer vernachlässigbaren Degradationsrate von $-0,2\%$ / Jahr, die andere mit einer Degradationsrate von $-0,69\%$ / Jahr, viel höher, aber immer noch kompatibel mit einer Garantie von 25 Jahren bei 80% der ursprünglichen Leistung. Nach 35 Jahren gibt es mehrere Mechanismen, die auf eine schnellere, nicht lineare Verschlechterung hinwirken. Trotzdem befinden sich die 21,5% der PV-Module immer noch in optimalem Zustand und können erneut installiert werden, um den nächsten Meilenstein zu erreichen: 40 Jahre Betrieb. Eine vergleichende Analyse vergangener und gegenwärtiger Technologien sowie der Lehren, die aus den Geräten von gestern gezogen werden können, wird diese Arbeit ergänzen.

Résumé

La centrale solaire photovoltaïque TISO-10 (Ticino SOLare), connectée au réseau en 1982, est la plus ancienne installation de ce type en Europe. Outre son âge, le système photovoltaïque TISO-10 est presque unique en son genre, puisque l'ensemble de 18 modules de référence a été testé en laboratoire à intervalles réguliers au fil des années avec un simulateur solaire et que toutes ces mesures sont traçables à celle originale du 1982. Les données obtenues à partir du système photovoltaïque TISO-10 sont ainsi devenues un ensemble extrêmement précieux de haute qualité, qui peut être utilisé pour extrapoler les courbes et les indices de dégradation à long terme des modules photovoltaïques qui composent le système. Deux groupes différents de modules PV peuvent être identifiés. L'un avec un taux de dégradation négligeable de $-0,2\%$ / an, l'autre avec un taux de dégradation de $-0,69\%$ / an, bien supérieur mais compatible avec une garantie de 25 ans à 80% de la puissance initiale. Après 35 ans, il existe de nombreux mécanismes qui travaillent ensemble vers une dégradation plus rapide que linéaire. Néanmoins, les 21,5% des modules PV ont toujours une forme optimale et peuvent être réinstallés en visant le prochain jalon: 40 ans de fonctionnement. Une analyse comparative des technologies passées et présentes et de ce que l'on peut apprendre des dispositifs d'hier complétera ces travaux.



Seite absichtlich frei



Contents

Summary	3
Zusammenfassung	3
Résumé	3
Contents	5
List of abbreviations	7
Introduction	8
Context	9
Motivation of the project	9
Approach and methodology	11
Description of the TISO-10 PV plant	12
Arco solar PV modules	12
Technology evolution	13
Operations	15
Dismantling of the system	15
Mobile laboratory testing and indoor flashers validation	16
Visual inspection (according to NREL/IEA PVPS Task 13 format)	18
Visual inspection: high resolution pictures	19
Evaluation of hot spots: IR pictures, electroluminescence and visual inspection cross check.....	20
Discussion of results	22
Traceability and consistency of electrical performance measurements over time.....	22
Performance distributions of the full set of modules	23
Soft and hard failures	24
Visual inspection results and degradation mechanisms	27
Encapsulant discoloration	28
Front delamination.....	30
Backsheet damage.....	32
Cell cracks	33
Internal circuitry corrosion	34
Hot spots	35
Burn marks	35
Junction box	36
Potential-induced degradation.....	37
Multiple degradation modes	38
Frequency of the degradation modes	39
Safety issues	39
Summary of visual inspection and safety related results	40



Conclusions and outlook	41
Publications [within the project].....	42
References	43
Appendix	45
Description of MBJ Mobile Flasher.....	46
A History Of Changes.....	48



List of abbreviations

SFOE	Swiss Federal Office of Energy
TISO	Ticino SOLare
PV	PhotoVoltaic
NREL	National Renewable Energy Laboratory
BOS	Balance Of System
PVB	PolyVinyl Butyral
EVA	Ethylene-Vinyl Acetate
UV	Ultra Violet
IEC	International Electrotechnical Commission
LCOE	Levelized Cost Of Energy (Electricity)
STC	Standard Test Conditions
IR	InfraRed
IV curve	Current-Voltage curve
R&D	Research&Development
ATR	Attenuated total reflection
FTIR	Fourier Transform Infrared Spectroscopy
MMF	MisMatch Factor
PDF	Probability Density Function
FF	Fill Factor
PID	Potential Induced Degradation
BS	Back Sheet
WL (test)	Wet Leakage (test)
VI	Visual Inspection
FMEA	Failure Mode and Effect Analysis



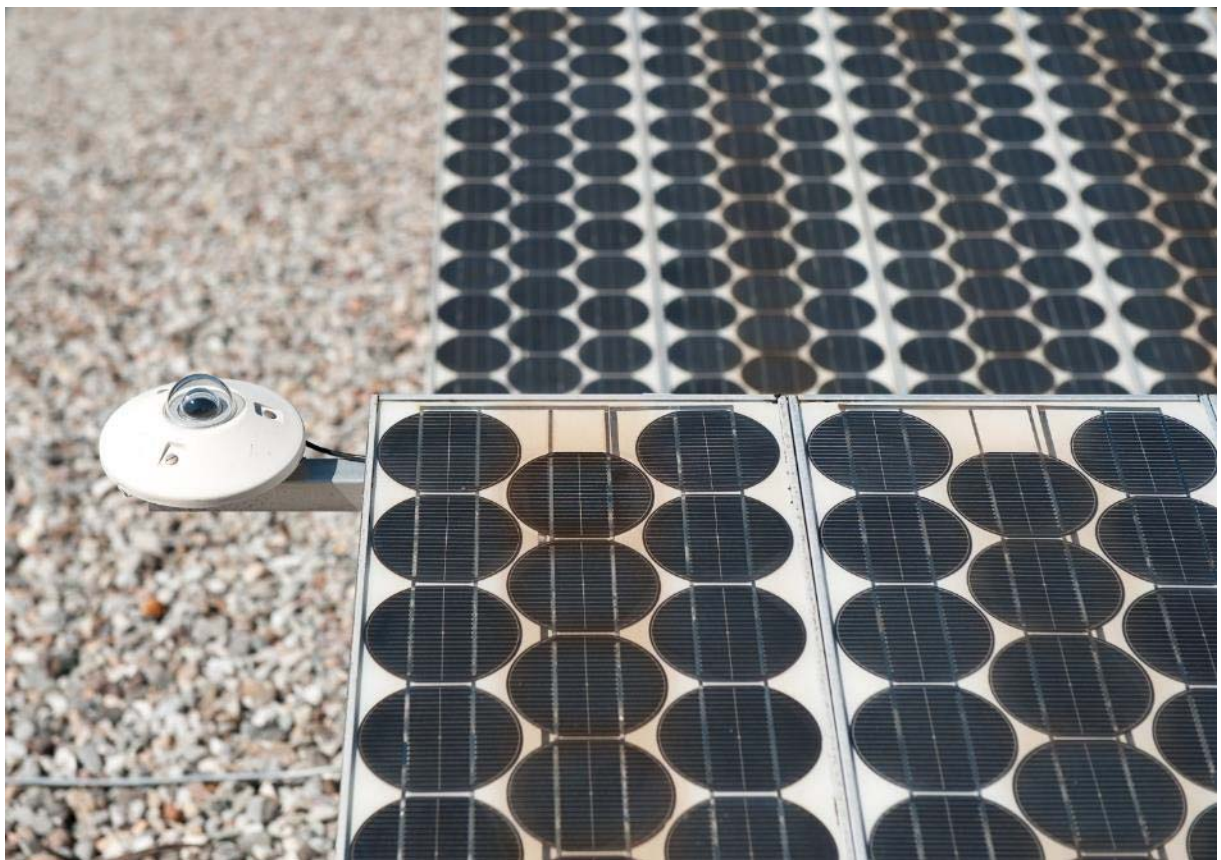
Introduction

The TISO-10 (Ticino SOLare) solar photovoltaic (PV) plant, connected to the grid in 1982, is the oldest installation of this kind in Europe. Since 1982 the plant underwent some configuration changes and a major refurbishment in 2010 when the plant was reinstalled (and “repowered”) in a new configuration on an adjacent roof, leading to a 10% increase in performance.

Besides its age, what makes the plant a unique of its kind is the fact that between 1982 and 2010 the performance (i.e. IV curves) of 18 selected reference modules were checked at regular intervals with high precision indoor measurements. Furthermore, two full testing campaigns were performed on the complete set of the 288 modules in 2001 and 2009/2010 with, performance verification, visual inspection and insulation testing.

In 2012, after the extensive measurement campaign of 2009/2010, an average degradation of the modules of the plant of 0.38 %/year was computed with a detailed data analysis [11], highlighting, however, the appearance of non-linear behaviours on the long-run.

Purpose of this work is to perform a “pre-final” check of the system, with a verification of the evolution of non-linearities and of safety aspects, further to a performance check and an update on reliability issues.





Context

Motivation of the project

In the run to cost reduction, the reliability and durability of PV systems is one important factor. The solar industry has answered to the questions on the performances' degradation of PV components, particularly modules, with the issue of international standards, to certify the quality of the products on the market. Even though the use of accelerated sequences is useful to check the limits of the different materials, the IEC standards are not meant to grant a minimum lifetime for the tested products: the interactions of different degradation factors follows complex dynamics and is far to be understood; the validation of accelerated testing through long term monitoring of PV systems is therefore crucial to set appropriate models to simulate the components' behaviour with respect to aging.

In a recent study by NREL (National Renewable Energy Laboratory) [11] a literature review of photovoltaic degradation rates resulting from almost 200 studies from 40 different countries has been published, where only few plants are more than 30 years' old.

Interestingly, it emerges that the quality of these data is often questionable: studies that used nameplate rating as reference, but used indoor solar simulators to verify degradation, showed less variation than similar studies using outdoor measurements, even when accounting for different climates.

The TISO-10 PV plant, further to be the first grid connected PV plant in Europe, is, in this sense, a unique-of-its-kind: a set of 18 reference modules has been tested indoors with a solar simulator at regular intervals over the years and these measurements are traceable to the original measurement performed at the Joint Research Centre (JRC) in Ispra, in 1981.

Moreover, all modules from the plants have been subjected to indoor laboratory measurements three times over the system's entire life.

As the research from NREL stresses, indoor laboratory testing is much more reliable in determining long-term degradation rates than data taken from outdoor monitoring, and only a reduced number of studies report degradation rates extrapolated from indoor laboratory testing: this makes, prospectively, the data that can be obtained from the TISO-10 PV system an extremely valuable data set of high-quality, which could be of great benefit to the whole PV community.

An additional unique asset of the TISO-10 plant is - contrarily to many other works in the literature - the fact that the full story of the PV system is well documented. So that, besides determining the long-term degradation rate of the specific module technology (crystalline silicon), additional information about the full system and the other components (inverters, monitoring system, BOS, etc.) and meteorological data, including light spectrum, are available.

Insights on wear-out mechanism: in 1980 ARCO Solar was the first manufacturer of solar modules to reach a manufacturing capacity > 1 MW per year; in 1997, under the name of Siemens Solar, it was the first company to release a 25-years-long module warranty. The ARCO Solar modules of the TISO-10 plant, installed in 1982, represent therefore one of the first industrial products available for a long term analysis - comparable to the warranty intervals - on the evolution of failures in a temperate climate. This is even more interesting when we consider that other plants, employing the same typology of modules, are still in operation in Italy and Sweden, under different climatic conditions.



An additional point of interest is that the modules of TISO plant witness completely different behaviours in terms of encapsulant yellowing. The phenomenon, far to be unknown, is still of great interest for the PV industry today: production of EVA formulas with focus on cost reduction, reduction of UV filtering of glass to increase efficiency and pass/fail criteria dictated by previous versions of IEC standards, where the UV test was not adequate to simulate real life exposition, might lead to a recrudescence of it. The introduction of BIPV modules, with higher module temperatures (thus higher risk of yellowing) and strict aesthetical requirements in terms of colour uniformity, confirm the interest to study and modelling the mechanism of yellowing in not accelerated conditions, not only for Ethylene-Vinyl Acetate (EVA), but also for PolyVinyl Butyral (PVB), which has been confirmed to be the encapsulant used for the lamination of TISO-10 modules [26].

Finally, obtaining information on wear-out mechanism is of paramount importance in determining the exact life of a PV system and, prospectively, in computing LCOE calculations on the cost of solar electricity over the entire life span of a system, which may have strong economic consequences.

Statistical assessment of safety in operation: another crucial point is the behaviour in terms of safety of the system. The thorough statistical analysis of hot spots and their origin, the verification of interconnector breakages, bypass diodes conditions, the mapping of delaminations, will help us to properly understand the status of the PV plant and to highlight the plus and the minus of the old technology with respect to the present ones, with particular focus on arcs and the related risk of fires. Ideally, PV modules in good shape could be sorted and reinstalled targeting the next milestone: 40 years of operation.

The aim of the whole project should be not only to take a complete picture of the status of the system at its end of life, but also to trigger new activities with a high resolution data set.

Some of the possible developments are:

- The use of digital pictures to train an artificial intelligence software to detect and classify defects,
- Modeling of failure modes, yellowing: manufacturing of different samples with the old encapsulant recipe, in order to perform laboratory accelerated testing and compare the results with long term testing experienced with TISO.



Approach and methodology

We have adopted the following strategy in order to achieve the expected results.

In order to determine quantitatively the maximum amount of information from the complete set of modules of the TISO plant, the following activities were envisaged.

- Dismounting of the full system from the roof of the building.
- Use of a mobile flasher (class AAA), metrologically aligned with the Pasan 3a/3b flashers, to perform simultaneously the:
 - Performance measurement
 - Electroluminescence test
 - Insulation measurement
 - Diode verification measurement

The use of a mobile flasher reduces considerably the effort for the full characterization of the complete set of 288 modules when compared to indoor lab testing.

- Additional performance measurements on the 18 reference modules with the Pasan 3B flashers in SUPSI PVLab and in JRC ESTI (used for the last historical series of measurements) in order to align the new measurements, performed with the mobile flasher, to the historical ones.
- Use of high resolution DSLR setup (36 Mpixel) to record repeatable images of front and back of all the modules. This data set will allow a complete traceability of the position and dimension of defects for a thorough visual inspection.
- Use of portable microscope to detail, with digital pictures, the interconnectors status and/or other defects.
- Use of the NREL/IEA PVPS Task 13 simplified format for the Visual Inspection of the complete set of modules in order to populate the international database with the results of an End Of Life PV plant.
- Use of wet leakage test to measure the insulation of the modules (depending on the effort it has to be decided if on all or part of the modules).
- Collection, organization and statistical analysis of the results:
 - quantification and statistical distribution of the degradation rates;
 - correlation between the module electrical parameters and the power loss in order to relate the degradation to specific failure modes (for instance, relating a reduction in fill-factor to failures in interconnections, or a reduction in short-circuit current to encapsulant yellowing).
- Check of the historical dataset format in order to:
 - compare the new measurements with the available ones going back to 1982
- Selection and sorting of the modules in strings to be mounted again for a project “Beyond 40 years”.



Description of the TISO-10 PV plant

The TISO-10 plant was installed on a flat roof of an educational building (presently belonging to SUPSI) and connected to the grid in Lugano on May 13, 1982. At the time, the plant was nearly south facing (azimuth = -4°) with a 60° tilt (55° since 1995) to maximize winter yield and reduce the impact of snow loads. Since then, the plant underwent a number of configuration changes and a major refurbishment in 2010, when the plant was moved and reinstalled in a modified configuration on the flat roof of an adjacent building and was finally reconnected to the grid in January 2011.

In the new configuration, the plant had an identical orientation but a lower tilt (20°). The repowering accompanying the relocation led to a + 10% increase in performance, mostly due to the re-sorting of modules into strings to minimize current mismatches. As reported in the previous study [1], which briefly recalls the history of the plant (together with other studies [14-21]), over the years, the changes have regarded mainly the substitution of the inverters that were changed four times (in 1992, 2003, and 2010) during the plant's operational life.

The climate in Lugano ($46^\circ 00'N$, $8^\circ 57'E$, 320 m above sea level for the test site) is moderate with monthly average temperatures ranging from $1.1^\circ C$ to $20.8^\circ C$ and a relative humidity (RH) between 57% and 80% (monthly averages). According to Köppen-Geiger classification, [22] Lugano has a subtropical climate ($-10^\circ C$ to $+35^\circ C$, with less than 90%), which is slightly mitigated by the presence of a lake and by the occurrence of moderate snow loads in winter. The cumulative annual global irradiance²³ at 45° tilt (azimuth = 0°) is 1240 kWh/m^2 .

Arco solar PV modules

The plant is composed by 288 c-Si modules (Arco Solar, ASI 16 2300) with a nameplate value (1000 W/m^2 and $25^\circ C$) of 37 Wp and total area efficiency η of 10%. Table 1 summarizes the technical specifications of the modules and solar cells as delivered by the manufacturer in 1981 (see existing studies [24,25]). The specifications indicate that the two layers of polymer foil used in module manufacturing in 1981 are Polyvinyl Butyral (PVB). In a personal communication, a former Arco Solar Manager confirms that, at the time, the encapsulant is likely to have been PVB and that three different suppliers of PVB were used by the company [26]. Furthermore, the three suppliers were using different chemistry and stabilizers, an information which was not available to the company at the time. A set of optical and chemical analysis (e.g. attenuated total reflectance—Fourier transform infrared analysis [ATR-FTIR]) performed in 2018 by a third-party laboratory confirmed that the encapsulant is made of the same base polymer (PVB) with the presence of different amounts and types of stabilizing additives. The analysis has been limited to three modules (out of 288), representative of three different classes of modules, with respect to their aging behaviour. In the following years, the production at Arco Solar switched from PVB to ethyl-vinyl-acetate (EVA), mostly for cost reasons. This is mentioned as well in a report by Ente Nazionale Energie Alternative (ENEA) (existing study [27]).

The use of a 3-mm thick tempered glass, of a Tedlar/metal-plate/ Tedlar backsheet and of a hot-melt butyl edge sealant makes the module sealing quite solid. For all modules, the metal plate of the backsheet is most likely a steel foil grounded to the frame, to avoid capacitive coupling and arching at high voltages. The junction box is a weather-proof plastic box hosting a bypass diode, and the mechanical stability of the module is reinforced using an anodized Al frame. Of the initial set of 288 modules, three devices were replaced in the initial months of operation while in warranty, and five modules have been replaced over the years with a set of spare modules. Information about the exact date of substitution is not available. Over the years, and for a smaller portion of the modules, the junction boxes, terminals, and connectors of some modules, when required, were repaired or replaced



to keep them operational. In 2003, the same modules (Arco Solar, ASI 16 2300) have been the subject of a similar study after 22 and 29 years of operation in central Italy [28,29].

Power/efficiency (nameplate)	37 W ± 10% (1000 W/m² and 25°C) η = 10% (total area) Voc = 21.5 V, Isc = 2.55 A, FF = 68%
Cells	4" wafers (Ø 102.5 mm) Mono-crystalline Si (Czochralski) Two ribbons/cell Thickness*: 320-330 µm (measured)
Module size	Area: 121.9 × 30.5 = 3'718 cm ² Depth: 3.8 cm (w. frame) Weight: 4.9 kg
Electrical layout	35 cells in series
Front glass	3-mm tempered
Encapsulant	PVB
Backsheet	Tedlar/metal-plate/Tedlar (the metal plate is likely steel for all/most samples)
Junction box	Weatherproof plastic box, hosting a bypass diode
Edge seal	Hot melt butyl
Frame	Full perimeter Al- frame
(*) Different cell thicknesses are provided in the specs: 9-12 mils (229-305 µm)	

Table 1: Solar cell and module specs [24,25]

Technology evolution

Over the last 35 years, the crystalline silicon (c-Si) wafer-based technology has clearly become the dominant technology in solar, with thin-film based solution suffering to gain considerable market shares. The c-Si technology has dramatically changed in these years in terms of the use/availability of materials, sizes, design practices, minimum quality and qualification requirements. In Table 2, we recall some key figures for the 80's and for year 2018, and give estimates for 2028, showing the evolution of the solar PV technology based on c-Si at market, cell and module level. Several of these changes have led - and will certainly lead - to improvements in the quality and lifetime of today's solar products, while others, considering the present cost-reduction market dynamics, may lead to a poorer durability of today's technology with respect to the technology of over three decades ago. Without going too much into detail in this work, a typical example would be the reduced cell thicknesses of the solar cells in use today, which makes them more prone to be affected by cracks during the transport and handling phases or during operation, with potential increased losses in safety and performance compared to the modules investigated in this work.



	Market			Cell					Module		
	Global shipments (GWp)	Global cum. installed capacity (GWp)	Module price (USD/Wp)	Active area (cm ²)	Dimension/ingot	Thickness (µm)	Busbar per cell	Cell type	Encapsulant	Module structure	Module power (Wp)
1980 Solar/ASI 2300-16	< 1 MW	-	35.4	81.6	Diam. 102.5 mm 4" ingot	320	2	Al-BSF	PVB, (later EVA)	Glass/ reinforced foil	37 (35 cells)
1980 Industry STD	<< 5 MW	~10 MW	> 35	78.5	4" ingot	350-450	2	Al-BSF	PVB, EVA, Silicone	Glass/foil Glass/glass	< 40
2018 Industry STD	120 * E 130 ** E	520 * E 530 ** E	0.34 [^]	243	156 x 156 mm ² 8" ingot	170-180	4 - 5	Al-BSF: 60% PERC: 30%	EVA >>90%	Glass/foil >>90%	280 (60 cells)
2028 Industry STD	743 * E 1792 ** E	4258 * E 7733 ** E	0.16* E 0.11** E	≥ 243	≥ 156 x 156 mm ² 8" ingot	130-150	5, 6+, no BB	BSF: 5% PERC: 65% SHJ: 15%	EVA: 70% PO: > 20%	Glass/foil: 60% Glass/glas: 40%	390 (72 cells)

Table 2: Technology evolution from 1980 to 2028

Market 2017: shipments ~100 GW, cumulative ~400 GW; E: estimates; * CAGR: 20%, ** CAGR: 30% (CAGR = Compound Annual Growth Rate)

Price: [^] 2017 year's end; 2012 actualized prices (1 CHF = 1.04 USD); Learning rate LR (1976-2018): 22.8% (i.e. price reduction of 22.8% for every doubling of cumulative shipments)

Technology: Al-BSF: Al Back Surface Field; PERC: Passivated Rear Emitter Contacts (includes PERT/PERL); SHJ: Silicon Hetero-Junction; PO: polyolefin Reinforced foil: Tedlar/steel/Tedlar with edge seal.



Operations

Dismantling of the system

The project has started at the beginning of October 2017, with the dismantling of all the 288 modules from the roof of SUPSI's Aula Magna. The position of the modules in the strings has been mapped before placing them on pallets for the transportation. Some pictures of the activity are presented here below:





Figure 1: ARCO Solar Module before/after the cleaning: negligible effect on performances.

As it can be seen from the pictures, the conditions of the modules were critical for the detachment of the Tedlar back foil and for the severe darkening of most of them. The modules were then placed under a roofed area to grant an easy accessibility to the mobile flasher.

Mobile laboratory testing and indoor flashers validation

The test activities were conducted by two operators, to optimize the flow and reduce at the maximum measurement time. After having checked that the temperature of the modules in the morning, at the starting of the activity, was around 10°C, it was decided to store them progressively in a temperature conditioned room, located next to the roofed area, in order to keep as near as possible to 25°C their temperature.

One of the modules was measured in the SUPSI PVLab with the Pasan 3b flasher in order to be used as reference for the system (Figure 3)

The mounting frame was properly adapted and the location of the module was constantly the same, in order to grant the repeatability of the measurement. The temperature of the module was further measured with a portable IR thermometer, in order to have 3 points of verification for more accurate temperature corrections.

All the 288 modules were measured according to the following test sequence:

- Electroluminescence image
- Power measurement (IV curve)
- Frame continuity measurement
- Insulation measurement
- Diode check

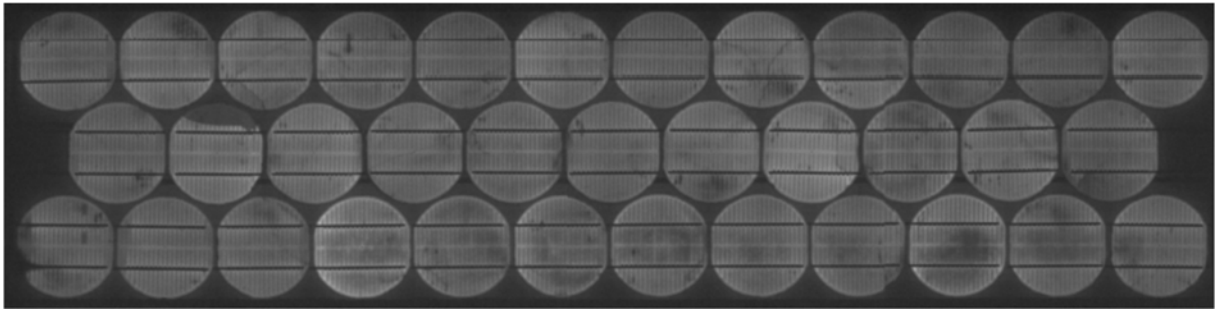


Figure 2: electroluminescence of MBJ's reference module 144185, see following page for electrical results

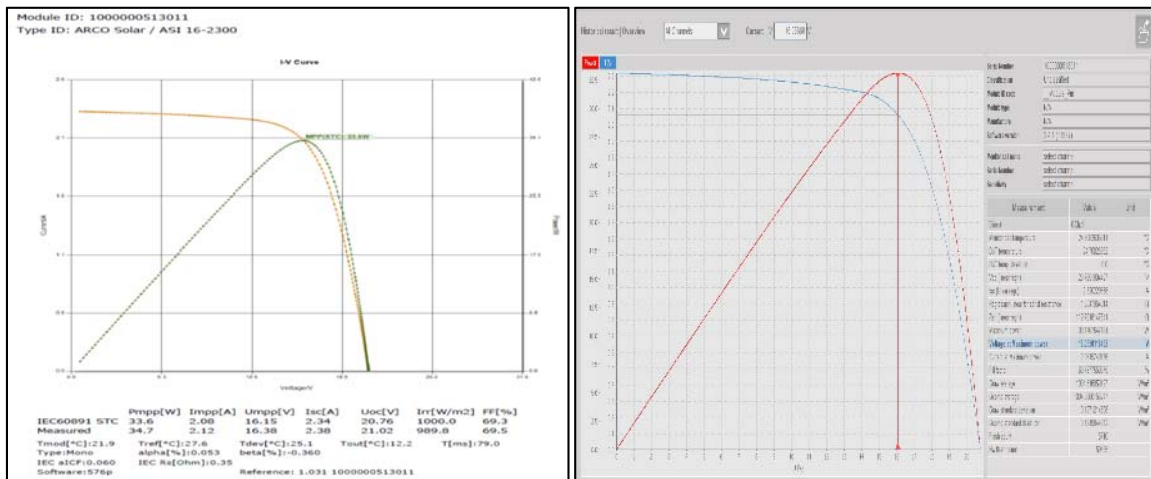


Figure 3: MBJ's reference module S/N 144185: power of 33.6W measured on MBJ (left) versus 33.1W of Pasan IIIb (right), 1.5% difference.

We will see in the next pages, that after 35 years of operation, the major part of the modules is still satisfying a 80% minimum power requirement, normally set by modern manufacturers after 25/30 years of life.

The measurement of 18 reference modules with Pasan 3b in SUPSI and Pasan 3b in JRC, with reference cells used in the past, gave confirmation from the metrological point of view on the good results from MBJ portable flasher.

A further empirical check was possible thanks to availability of a module not exposed outdoor, with serial number 144482.



Visual inspection (according to NREL/IEA PVPS Task 13 format)

After the electrical characterization, all the modules were visually inspected following the VI legenda proposed by NREL in conjunction with IEA PVPS Task 13 experts, to standardize the findings on modules exposed in the field.

Within this activity, which involved 4 trained persons, the sorting of the modules was performed according to three different categories, based upon the yellowing of the encapsulant.

Class "A": total white module

Class "B": partially yellowed module (particularly in the central cells' row)

Class "C": totally yellowed module

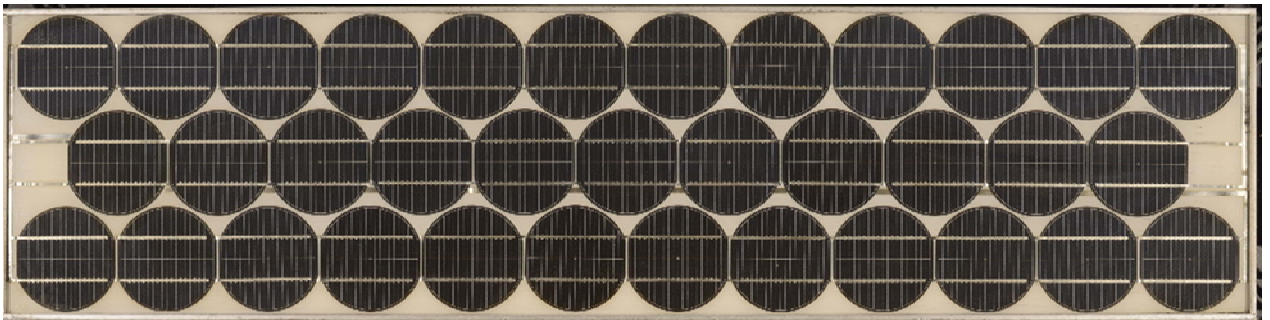


Figure 4: Class A module: clear encapsulant

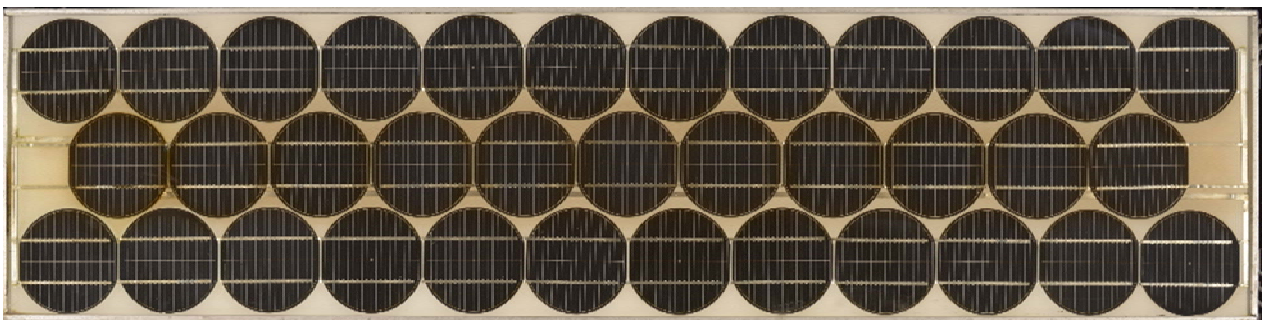


Figure 5: Class B module: central cells' row partial yellowing

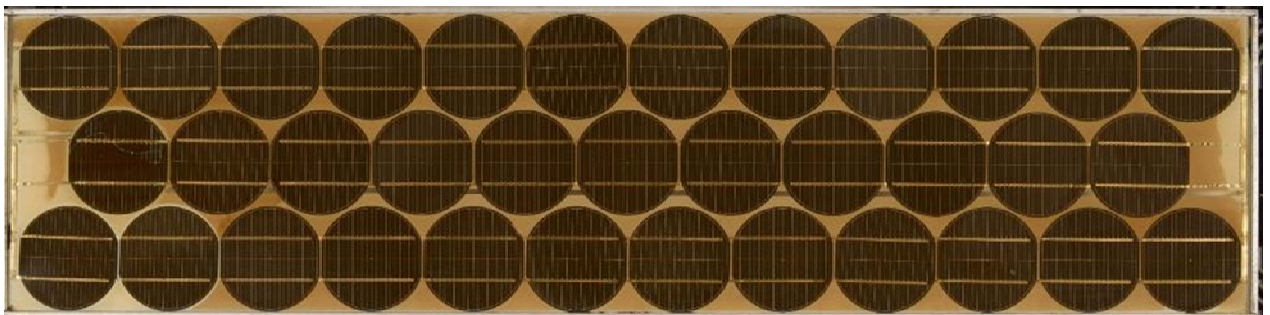


Figure 6: Class C module: complete yellowing



A detailed qualification report from JPL on the ASI 16-2300 type [25], referring to serial numbers falling between the ones of the TISO, gives evidence on the use of PVB for the production. Further to visual inspection, all the 18 reference modules, monitored since the beginning in terms of periodical indoor power measurements, initially at JRC Ispra and afterwards at SUPSI, were grouped and prepared for further verifications in the two institutes.

Final Design Modules*												
SERIAL NUMBER	TEST VOLTAGE, VOLTS		I (TEST), AMPS		POWER, WATTS		GROUND, A		ISOLATION, A		ENVIRONMENT, P/P	
	PRE	POST	PRE	POST	PRE	POST	PRE	POST	PRE	POST		
1	143316	17.32	17.23	2.04	2.02	35.26	34.80	0	1	5	10	PASS
2	143320	17.32	17.23	2.03	2.01	35.21	34.63	0	1	4	7	PASS
3	143322	17.32	17.23	2.05	1.94	35.71	33.43	0	0	4	10	PASS
4	143323	17.32	17.23	1.98	1.96	34.24	33.77	0	0	4	6	PASS
5	143324	17.32	17.23	1.95	1.92	33.69	38	0	1	4	6	PASS
6	143328	17.32	17.23	1.95	1.94	33.82	33.43	0	0	5	8	PASS
7	143331	17.32	17.23	1.97	1.94	34.07	33.43	0	0	4	13	PASS
8	143334	17.32	17.23	1.95	1.92	33.72	33.08	0	0	5	7	PASS
9	143337	17.32	17.23	1.99	1.96	34.43	33.77	0	0	4	6	PASS

*Features Include:
1. Grounded Steel Foil
2. VAMAC Edge Sealant

Figure 7: Data from original qualification of ARCO Solar ASI 16-2300 modules in 1981. The serial numbers of the panels installed in the TISO PV plant include 2 modules with S/N 143287 and 143407, practically of the same lot; the electrical parameters of these modules are aligned to the measurement performed in JRC in 1982 on the TISO modules.

Visual inspection: high resolution pictures

After the complete visual inspection all the modules were photographed with a Nikon D800 high resolution digital reflex camera mounted with a glass reflection free setup, in order to record the maximum possible detail of each component. The white balance was accurately measured in order to trace quantitatively the yellowness of the modules and compare it to future evolutions for the modules mounted on the field to go beyond 40 years.

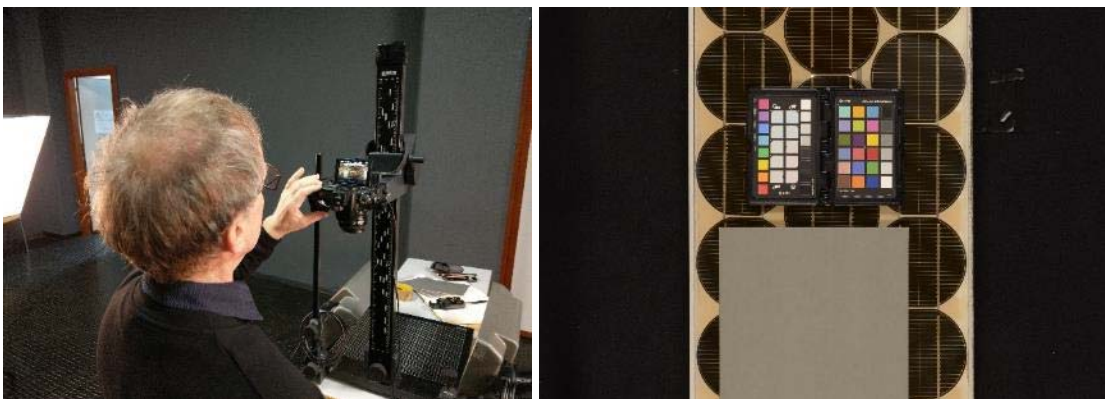


Figure 8: Preparation of photo setup , colour checker and grey cardboard for precise white balance definition

The picture data set was completed with macro pictures and digital microscope frames, with a detailed documentation of the recurring defects of the modules. In the following pages, some examples are detailed, together with the discussion of the impact of each defect on safety.



Evaluation of hot spots: IR pictures, electroluminescence and visual inspection cross check

The evaluation of the hot spots on the 288 modules of the TISO plant has been performed through the analysis of the electroluminescence pictures shot during the measurement campaign with the MBJ portable flasher, followed by a comparison with visual inspection results and a cross check on a representative sample of 10 modules, analysed with indoor and outdoor IR thermal camera.

The first step consisted in the selection of modules with visible cracks and well recognisable defects, highlighted by drastic differences in the luminescence of the EL picture. Second step was the comparison of these areas in terms of browning, delamination, bubbles, due to the heating process behind the hot spot: this task was accomplished using 36 Mpixel high resolution images, shot in the dark room with controlled and reproducible light exposure. This process allowed to discriminate between different types of defects (cracking, delamination with moisture penetration, soldering defects, etc.) which were subsequently analysed through the IR images taken indoor, using a power supply to force current through the cells. In order to highlight gradually the temperature differences on the modules, the procedure described in the white paper “Review on Infrared and Electroluminescence Imaging for PV Field Applications” was applied: infrared shots were taken with a Fluke IR camera, with resolution of 320x200 pixel, at the beginning of current flow, after 20”, after 120” and after 4 minutes, once reached the thermal balance. Though the same patterns of the EL pictures were highlighted on severely damaged modules, the condition of the solar cell in front of the junction box was not clear: apparently, one of the most critical cells was only partially hot, even when important defects from the electroluminescence and visual inspection pictures were evident. To have a better understanding, it was decided to further check the same modules also in outdoor conditions, with IR analysis through direct current generation of the module, which was exposed in short circuit mode.

This analysis allowed to recognize 78 modules with critical hot spots (temperature difference $>20^{\circ}\text{C}$) and 110 modules with light hot spots ($10^{\circ}\text{C} < T < 20^{\circ}\text{C}$); 85 modules showed no sign of appreciable hot spot and 15 couldn't be inspected with the electroluminescence/IR test.

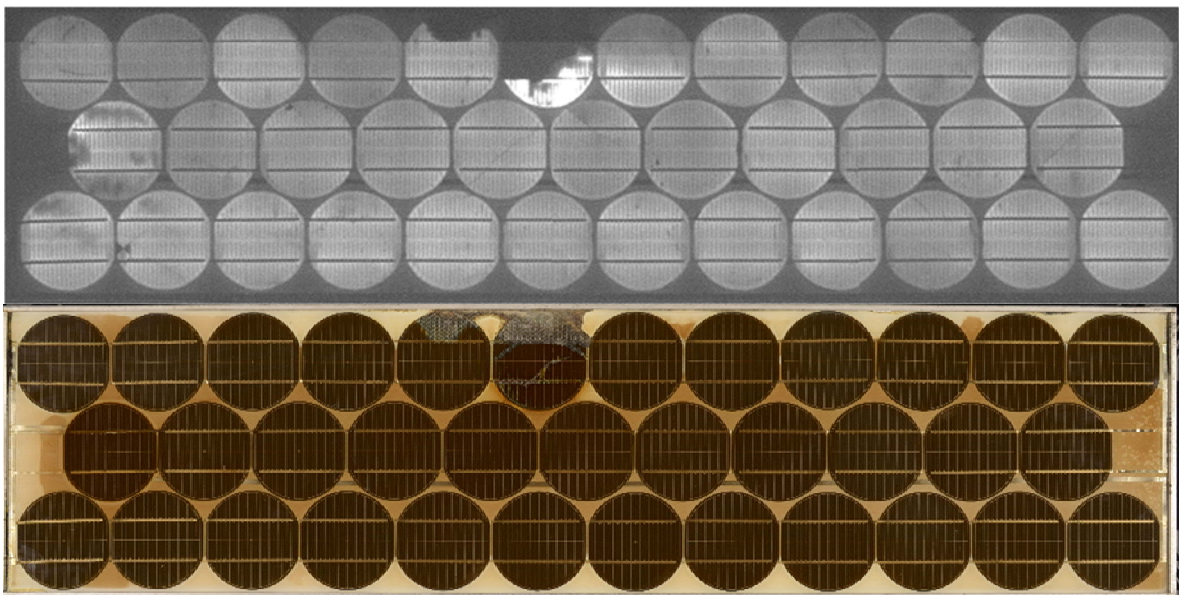


Figure 9: comparison of EL picture with visual inspection through high res image analysis

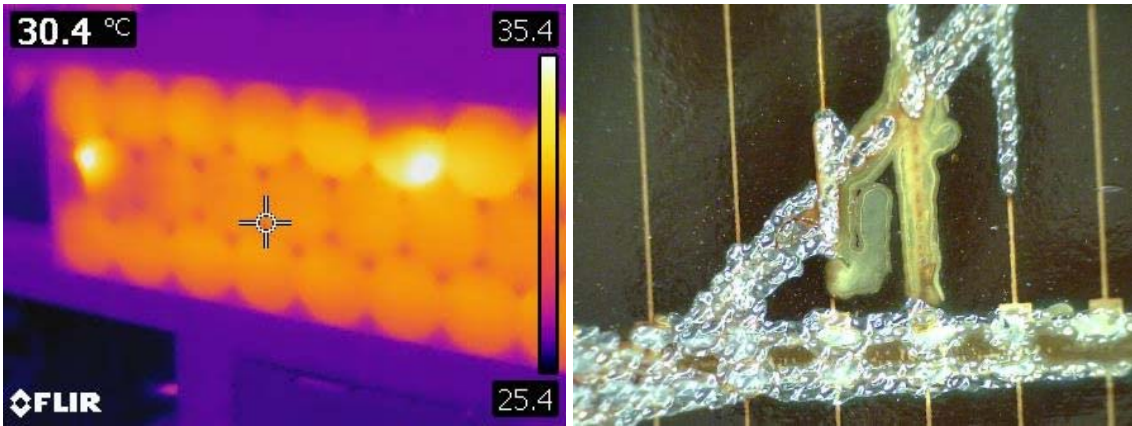


Figure 10: verification of EL results through indoor hot spot test, macro picture of hot spot area.

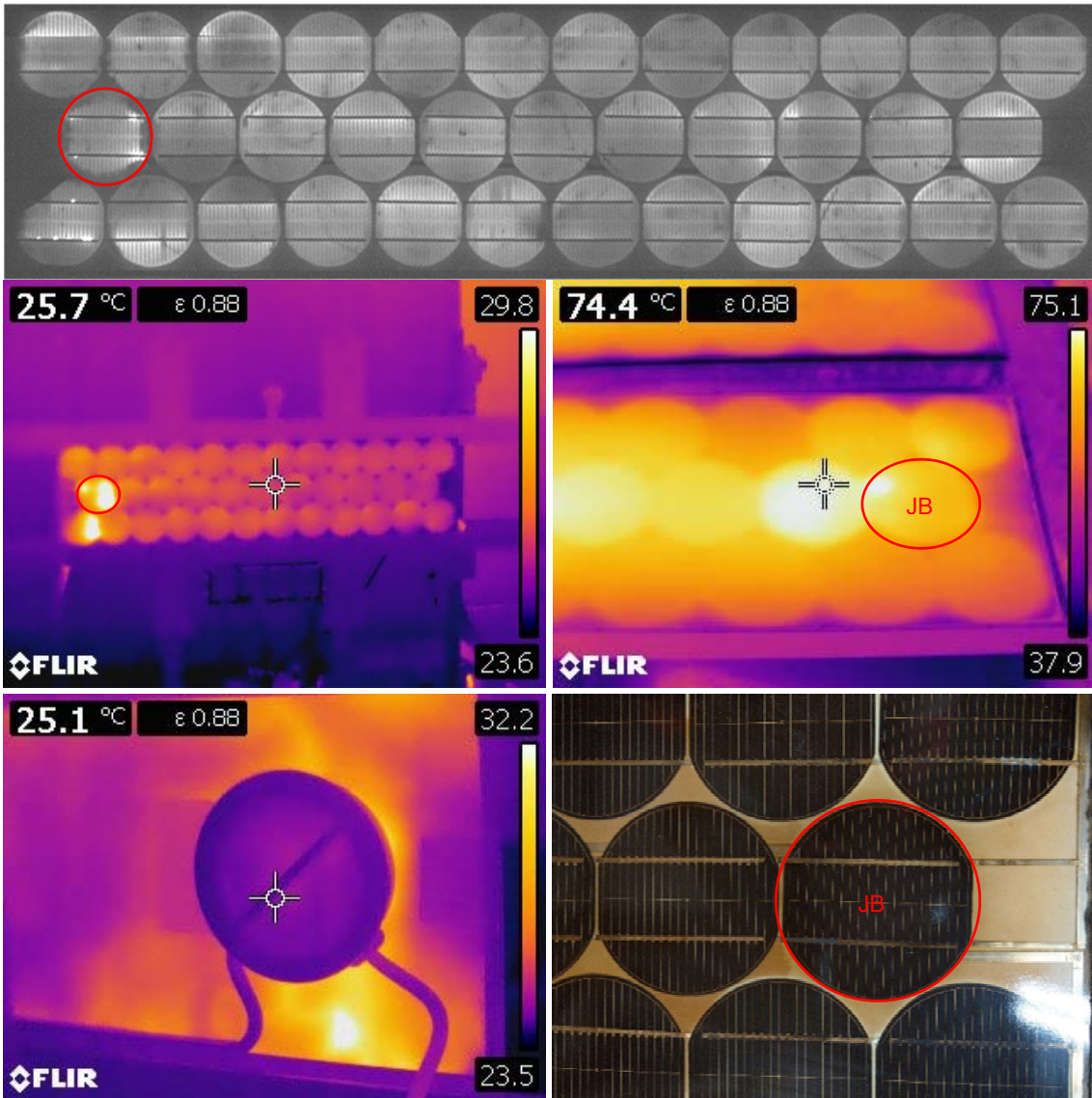


Figure 11: Comparison of Indoor (up, left) and outdoor IR (up, right): heating of the cell in front of the junction box is confirmed, different heat distribution is also clear. Below: indoor IR picture of JB (left) and Visual Inspection (right).



Discussion of results

Traceability and consistency of electrical performance measurements over time

As previously mentioned, the full set of modules belonging to the TISO 10-kW plant is made of 288 devices. The full set of modules have been characterized indoors in a controlled laboratory environment in years 2001, 2011 and 2017, while a sub-set of 18 reference modules – fielded with the rest of the modules - have been characterized at shorter intervals starting in 1982. Over the years, the measurements on the reference modules have been performed at different labs and using different measurement set-ups. Nevertheless, maximum care has been given to guarantee the continuity and traceability of the measurements and align the results obtained with the different setups over the years as synthesized in the table below.

ID Code	Serial Number	Power W (MBJ) 2017	Power W (JRC) 2018	Variation % (MBJ/JRC)	Variation % JRC ^a (2017/1982)
TEA1	142796	26.1	26.06	0.2	-26.7
TEA2	143069	30.61	30.3	1.0	-14.8
TEA3	144004	29.33	28.55	2.7	-19.7
TEA4	144291	29.61	28.69	3.2	-19.3
TEA5	144377	32.45	32.02	1.3	-10
TEA6	145113	27.36	26.77	2.2	-24.7
TEA7	145711				
TEA8	146689	26.92	26.1	3.1	-26.6
TEA9	146872	14.93	15.39	-3.0	-56.7
TA10	147216	30.56	30.59	-0.1	-14
TEB7	143073		33.7	-	-5.2
TEB1	143081	29.3	29.58	-0.9	-16.8
TEB2	143215	27.75	27.82	-0.3	-21.8
TEB5	143695	29.67	29.66	0	-16.6
TEB6	143743	27.73	30.6	(-9.4)	(-13.9)
TEB8	144311	29.05	29.27	-0.8	-17.7
TEB4	145693	27.91	28.44	-1.9	-20
TEB3	147591	28.55	28.87	-1.1	-18.8
Average deviation				-0.2%	-20.2%
Average deviation without outlier (in brackets and bold)				0.39% ^a	-20.6%

^aInitial 1982 reference value for all modules $P_{max} = 35.56$ W (see Section 5.1 and Table 4).

^bAverage deviation MBJ/JRC: $P_{max} = 0.39\%$; $I_{sc} = -1\%$, $V_{oc} = -0.02\%$, $FF = 1.35\%$.

Table 3: Comparison of the IV measurements (power) performed in 2017 on the set of 18 reference cells to align the measurement chains of the MBJ mobile lab LED-based and Joint Research Centre's (JRC's) Pasan III B flashers. The variation between the JRC measurements performed at JRC in 2018 and 1982 is shown as well.

If we compare the results obtained for the 16 reference modules (two are not in operation any longer), we observe that the discrepancy in the measured power falls within three categories: less than or equal to $\pm 2\%$, $\pm 2\%$ to 3% , and $\pm 3\%$ to 4% for, respectively, 10, two, and three modules. If we compute the average deviation for the power measurements performed with the two different set-ups (MBJ vs JRC) for all 16 modules and exclude one outlier, we observe an average deviation of $+0.39\%$ (MBJ/JRC), which leads us to the positive finding that the two measurement set-ups used in 2017 and 2018 are well aligned.



Finally, as a final mean of verification of the traceability of JRC's measurement set-ups over the years (1982 vs 2018), an Arco-Solar module not belonging to the plant, but of the same type and series of the modules investigated in this work (serial number 144482), has been flashed at JRC in 2018: the measured power of this module in 2018 corresponds to 34.55 W (no MMF applied), a value that lies very close (i.e. -2.8%) to the average value of the original 1982 P_{\max} measured for the 18 reference modules of the plant (i.e. 35.56 W). This value rather than the nameplate values (ie, 37 Wp) was used to compute the degradation rates for the measurements performed in later years of which we will discuss in the next paragraph.

Performance distributions of the full set of modules

The original probability distribution function for the performances of the full set of modules, based upon the analysis of the reference modules, shown in Figure 12 on the left, was a Gaussian, while the results of a later characterization campaign performed in 2001, after 19 years of field operation of the modules, show a transformation into a modestly left-skewed distribution, which we de-convolute in two subgroups described by two Gaussian distributions.

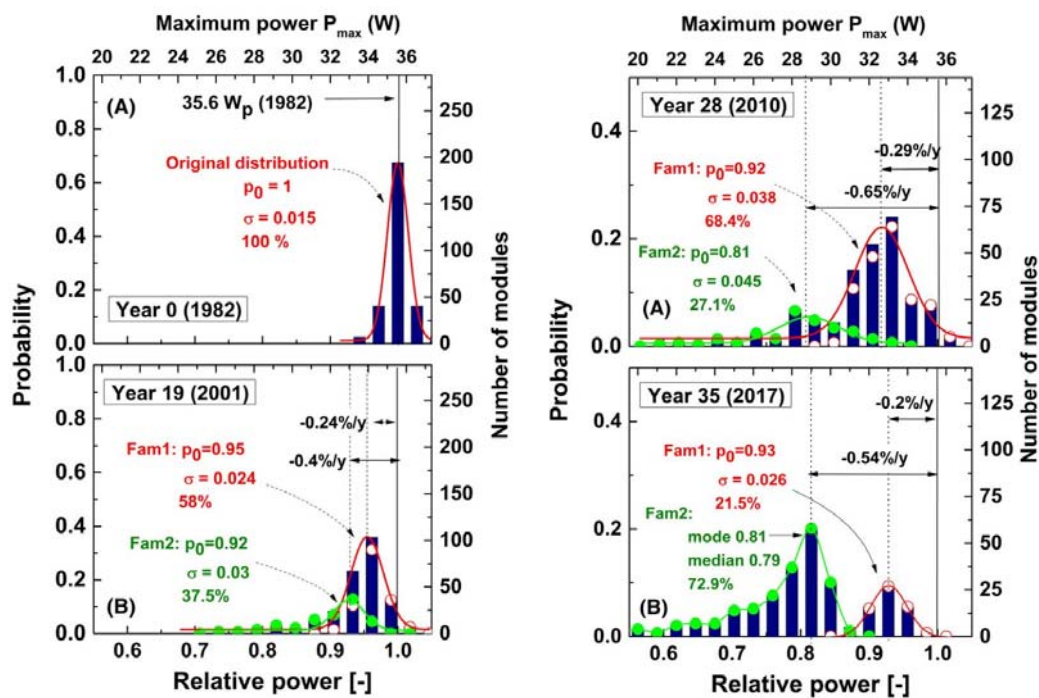


Figure 12: distributions of the power measured during the years on the modules of TISO. 1982: 18 reference modules. 2001, 2010 and 2017: full set of 288 modules.

One Gaussian is relative to a majority of the module's population (group 1, $\sim 58\%$) with a yearly performance degradation rate of $-0.2\%/y$ and the other (group 2, $\sim 37.5\%$ of the total) with a twice as large degradation rate of $-0.4\%/y$. The standard deviation of the two distributions is similar. Thirteen modules (group 3, 4.5% of the total) were not performing any longer ($P = 0$ W) in 2001, a share that increases to 15 modules ($\sim 5.2\%$) in 2017. Generally, these modules have a detached junction box or loss of continuity in the electrical circuitry. The performance measurements of 2010 (after 28 years of operation) are presented in Figure 12 on the right and clearly show that the earlier assumption of having



two groups of modules with different long-term performance behaviours is correct. The share of the two populations remains mostly unchanged:

1. Group 1: 68.4% of the module shows a very modest degradation that is well described by a Gaussian with mean yearly power degradation of $-0.29\%/y$;
2. Group 2: 27.1% of the modules can be described by a similar but broader distribution with a mean yearly degradation rate of $-0.65\%/y$.

Compared with the same values in 2001, for both families, the average yearly degradation rates in 2010 have increased. This observation is consistent with the growth in the degradation rates that can be inferred for the 18 reference modules.

From 2017 measurements, it becomes evident that a considerable increase in the degradation rates is happening over the last 7 years and that the Probability Density Functions (PDFs) are changing:

1. Group 1: 21.5% of the modules show a very modest degradation that is still well described by a Gaussian distribution with mean yearly power degradation of only $-0.2\%/y$.
2. Group 2: 72.9% of the modules are described by a negatively skewed distribution with a long tail described by mode ($-0.54\%/y$), median ($-0.62\%/y$), and mean ($-0.69\%/y$) values.

Soft and hard failures

The PDF of the module performance in 2017 can be correlated to the classification used in previous works of modules affected by **soft** and **hard failures**. Two examples for soft and hard failures can be found here below in Figure 13.

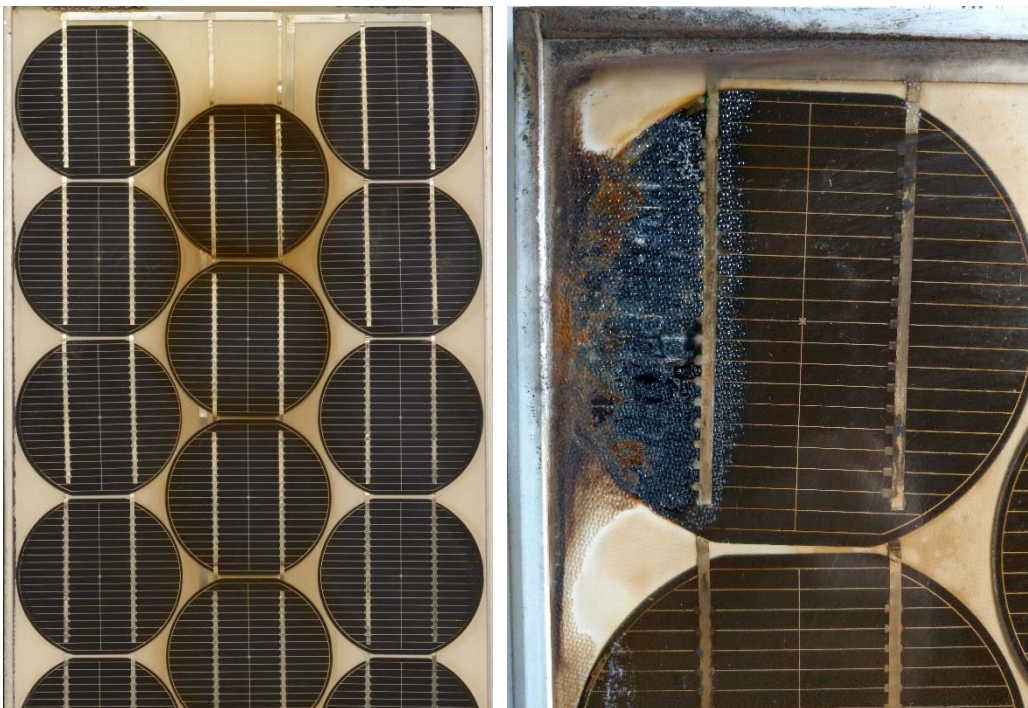


Figure 13: Soft defect (Left): yellowing of the central cells row; hard defect (right): delamination and corrosion of solar cell.

A detailed review and classification of the main failure modes, following an extensive and detailed visual inspection and other characterization means, is given in the coming pages, where particular emphasis is put on safety aspects as well. In Figure 14, we plot the relationship between losses in



module's power correlated to losses in V_{oc} , I_{sc} , and FF for the full set of modules in operation (288-13=275) and years 2010 and 2017.

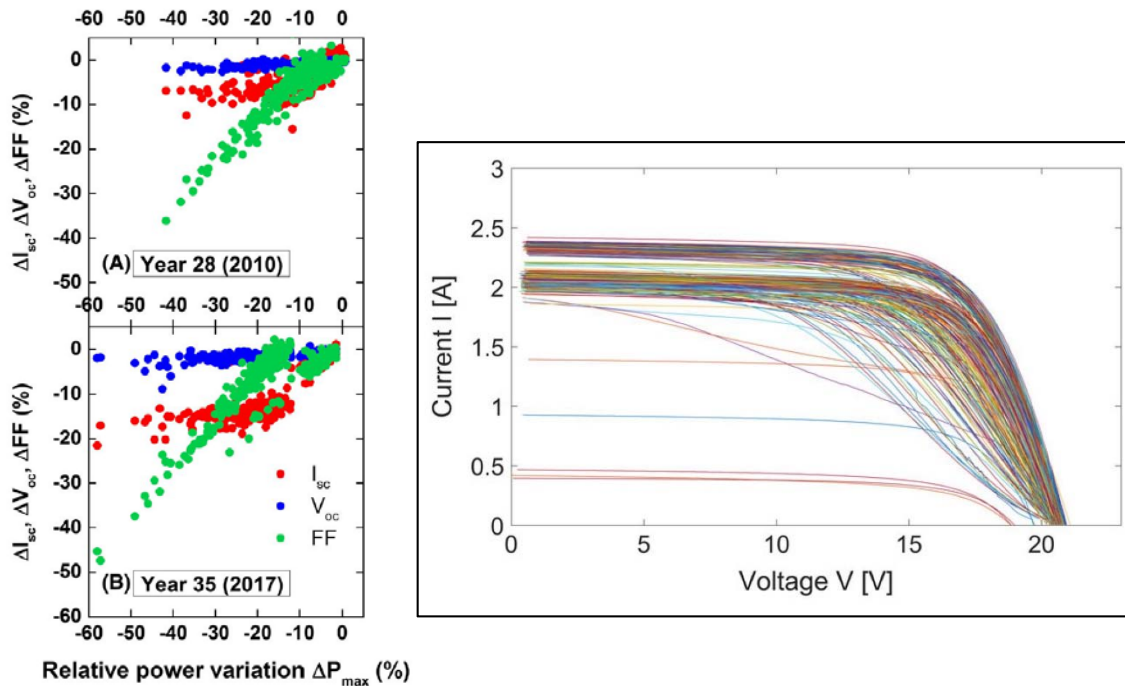


Figure 14: Left: relationship between the variations in P_{max} and the variation in I_{sc} , V_{oc} , and FF for the full set of modules, with respect to the original (1982) PV parameters, for years A, 2010 and B, 2017. Right: IV curves measured in 2017 for the 273 modules still in operation.

To compute these degradation rates, we use as the initial values the mean PV parameters measured in 1982 for the sub-set of the 18 reference modules.

In 2010 (after 28 years of operation), power losses can be clearly correlated to reduction in FF. In particular, large losses in P_{max} are mainly related to large losses in FF. No modules are affected by significant V_{oc} reduction, consistent with the fact that no interruption of the electrical circuit can be detected for the modules in operation, nor any potential-induced degradation (PID) was observed. A considerable fraction of the modules, on the other hand, exhibits losses in I_{sc} , which range between -5% and -11%. These modules are mostly affected by severe yellowing, minor delamination, and hotspots. In 2017 (after 35 years), the situation changes considerably and the trend of the relationship between P_{max} losses and FF losses is not proportional anymore. The two families identified in Section 5.2 for 2017 are clearly distinguishable in Figure 14, B. The modules belonging to Family 1 (with an average power degradation of -7%) are mainly represented by the cloud at the right-side of the plot, and experience a combination of moderate losses in FF and I_{sc} . Modules in Family 2, instead, show a more varied behaviour. With respect to 2010, modules with FF variations in the range $-10\% < \Delta FF < 0\%$ may show here P_{max} degradations of up to -27.3%. This shift is due to an increased reduction in I_{sc} with respect to 2010. This effect becomes particularly manifest if we observe the group with power losses between -12% and -17%, for which the degradation in P_{max} can entirely be ascribed to losses in I_{sc} . In Figure 14, on the right, we display the IV curves measured in 2017 for the 273 modules still in operation, where these different groups of modules can be directly distinguished.



Figure 15 shows the frequency of variations in I_{sc} and FF referred to years 2010 and 2017. In 2010, only 1.1 % of the modules showed I_{sc} losses higher than -10% (with an average of -4.7%), while, in 2017, this share of modules increased to 74.9% (with an average I_{sc} loss of -11 %). Conversely, the frequency of FF losses remains relatively unchanged from 2010 to 2017, with mostly an increase in the percentage of modules having strong FF losses (higher than -40%). A small number of modules results to have positive I_{sc} or FF variations, which we can attribute to uncertainty in the measurements and to the fact that the initial values used to compute the degradation rates refer to the averaged values measured in 1982 for the set of 18 reference modules. The reasons for this evolution in current losses will become clearer in the next paragraph. We suggest, however, that they are correlated to strong browning of the encapsulant, to the presence of hot-spots and cracked cells, and to delamination of the front encapsulant layer. Understandably, some modules are affected simultaneously by multiple failure modes (see Figure 13– right).

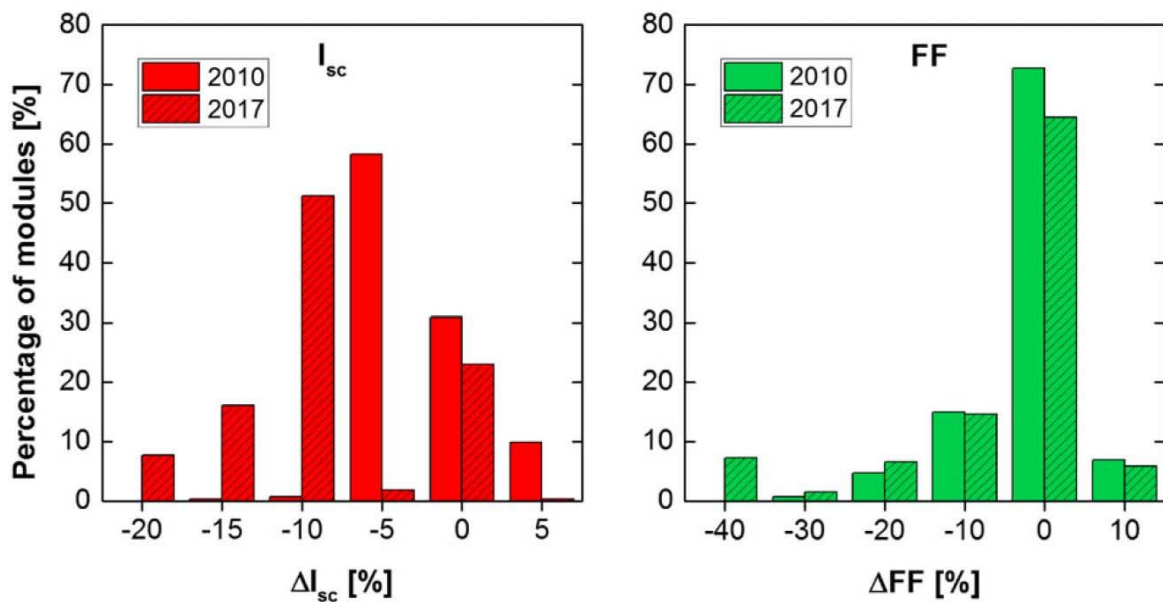


Figure 15: Histograms of the variation in I_{sc} and FF in 2010 and 2017 (with respect to the original 1982 PV parameters) with the percentage of modules corresponding to each bin.

By comparing the information contained in Figure 12 right, (a) and (b), Figure 14 left, and Table 4, it is clear that between 2010 and 2017 an acceleration in the aging of the modules is taking place for the majority of the modules, and we cannot exclude that the degradation rates will increase further in the coming years. Nevertheless, if we focus our attention on the 2017 “picture” and we consider the -20% threshold generally used to determine the life-time of the modules, we can conclude that after 35 years of operation in a temperate climate:



Year >	1982	2001 (19 y)	2010 (28 y)	2017 (35 y)
Modules (%)	288	288	288	288
PDF	Gaussian (*) Mean: 35.56 W _p Standard deviation: ±0.67 W _p (±1.88%)	1. g1–Gaussian: 189 modules (65.6%) Mean: -4.53%-0.24%/y 2. g2–Gaussian: 86 modules (29.9%) Mean: -7.15%-0.4%/y 3. g3–module at 0 W13 modules (4.5%)	1. g1–Gaussian: 191 modules (66.3%) Mean: -8.2%-0.29%/y 2. g2–Gaussian: 84 modules (29.2%) Mean: -19%-0.65%/y 3. g3–module at 0 W13 modules (4.5%)	1. g1–Gaussian: 62 modules (21.5%) Mean: -6.7%-0.2%/y 2. g2–left skewed: 210 modules (72.9%) Mode: -18.6%-0.54%/y Median: -21%-0.62%/y Mean: -24%-0.69%/y 3. g3–modules at 0 W15 modules (5.2%)

Table 4: Overview of the probability density function's (PDF's) and groups (g) describing the decrease in performance of the modules belonging to the TISO 10-kW plant over the years

(a) All modules belonging to Group 1 (62 modules, 21.5% of total) experience a degradation of at most -13% (mean: -6.7%);

(b) If we consider Group 2 described by a left-skewed distribution (210 modules, 72.9%) with a median set at 79 % (i.e. degradation of -21%), we observe that half of the modules belonging to this group (105 modules) has a maximum degradation that falls within the -20% boundary. If take into account a measurement uncertainty of ± 3% (for the MBJ flasher), this group would be even larger (i.e. 139 modules).

(c) We now combine the number of modules with power losses within the -20% threshold (62+105 = 167) for both classes. After 35 years of operation in a temperate climate, we can conclude that ~60% (167/288=0.58) of the modules would still satisfy a performance warranty that module manufacturers are presently considering to apply to the technology of tomorrow: i.e. 35 years of operation with maximum power losses set at -20% of the initial performance. If we consider a measurement uncertainty of ± 3%, the share of modules compliant with such a warranty would be 70%.

Visual inspection results and degradation mechanisms

In this paragraph the results of the extensive characterization of the modules performed based on the detailed visual inspection analysis and on the IV curve measurements are presented together with the degradation mechanisms affecting the PV modules. This information is complemented by the use of electroluminescence and infrared imaging. When possible, we try to correlate module performance losses to specific failure mechanisms. Further, additional potential safety threats are investigated by measuring the frame continuity, the functionality of the by-pass diodes, and the insulation of the modules.

Further to the 58% of modules still performing above the 80% of the initial power discussed in the former paragraph, the number of modules affected by catastrophic failures and not working any longer is limited to 15 (i.e. ~5.2% of the total): these modules generally present a detached junction box or loss of continuity in the electrical circuitry. In this section, we first describe the single failure modes observed, we then illustrate an example of a module affected by multiple failure modes, and conclude the performance degradation analysis by presenting the frequency of occurrence of the various failure modes; finally, we show the results of the safety tests.



Encapsulant discoloration

As shown in Par. 0, the most noticeable aging effect is a colour changing and loss in transparency (yellowing) of the encapsulant. Interestingly, this degradation mode did not affect all the modules to the same extent. Three classes of modules can indeed be identified (see, and):

- Class A (Figure 4): the encapsulant of these modules remained fully transparent.
- Class B (Figure 5): some modules show a moderate and localized yellowing, which generally affects only the central string of cells. Often, this effect is more pronounced in correspondence with the cell located over the junction box, most likely because of its higher operating temperature with respect to the surrounding ones.
- Class C (Figure 6): for this sub-set of modules, a uniformly distributed and pronounced browning is present over the whole surface of the device.

As we observed in the former paragraph, the reduction in I_{sc} is one key factor in the evolution of the performance degradation of these modules. In the last part of the system life, the average I_{sc} of the modules underwent an important deceleration, going from -4.70% in 2010 (i.e. after 28 years of exposure) to -11% in 2017 (i.e. 35 years). This is the result of different degradation mechanisms, the most relevant one being undoubtedly the considerable worsening in encapsulant yellowing, which in some modules turned to a uniform browning. Other factors contributing to the reduction in I_{sc} are the delamination of the front encapsulant layer and the presence of cracks that completely isolate portions of some cells, and will be addressed later.

The impact of the discoloration extent is clear in Figure 1, where modules in Class C (uniform browning) show on average the strongest power loss (-26.1% with respect to the initial values). It is remarkable that modules in Class A (for which the encapsulant is still fully transparent) are still performing, in average, at 95.1% of their initial power after 35 years of operation, corresponding to an average degradation rate as small as 0.14%/y.

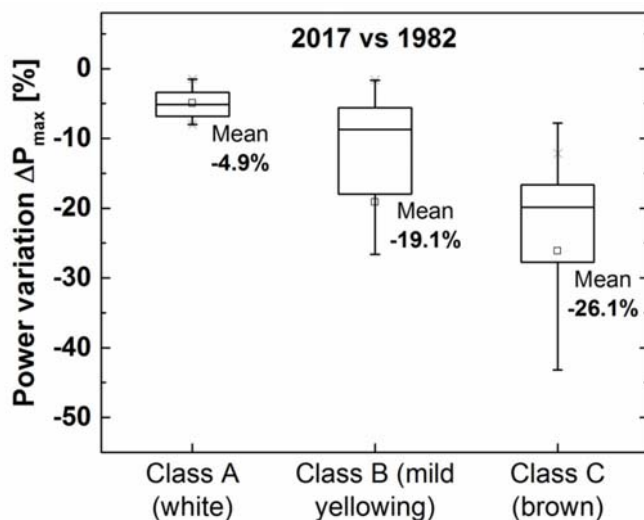


Figure 16: Power variation (2017 vs 1982) for modules belonging to the three classes defined based on the different level of encapsulant discoloration. The two regions in the boxes depict the first and third quartile, with the internal line indicating the median. For each box, the mean value is reported, and represented as a small square inside the box.

The relationship between power loss and the other electrical parameters (I_{sc} , FF, and V_{oc}) is shown in Figure 14 left for years 2010 and 2017. Here, we rearrange the plot for 2017 in order to investigate if a correlation exists between performance degradation and the three classes of modules (i.e. with



different encapsulant formulations). To avoid data overlap, we plot the values for Classes A and C in Figure 17 a), while modules of Class B are plotted in Figure 17 b).

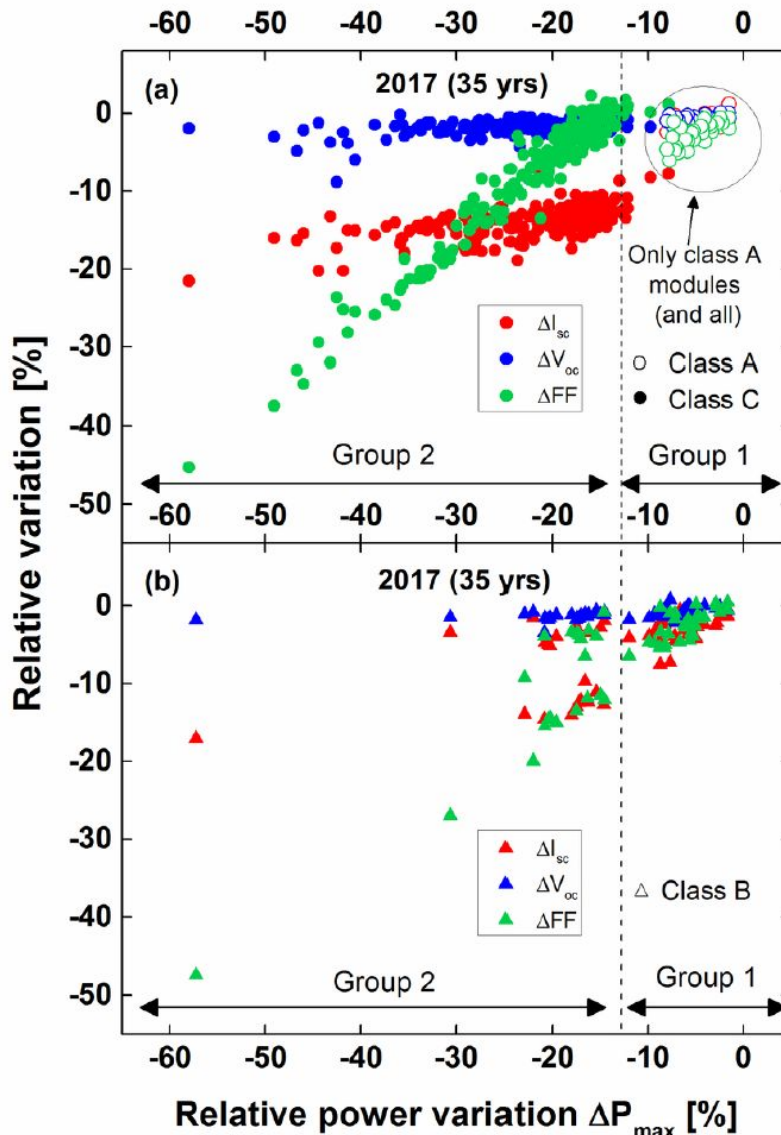


Figure 17: Relative variation of power (2017 vs 1982) for the full set of 288 modules and correlation to losses in V_{oc} , FF, and I_{sc} . a) Open circles represent Class A modules (still transparent encapsulant), full circles: are for Class C modules (browning or uniform yellowing). b) Class B modules (localized and mild yellowing). The vertical dashed line, at $\Delta P = -12.8\%$, indicates the separation between the two groups.

Consistently with what discussed in the previous paragraph, we distinguish the two groups, Group 1 and Group 2, corresponding to the two sets of modules that experienced a mean power degradation of 0.20%/y and 0.69%/y, respectively. The dividing line between the two groups is at -12.8% of relative power variation (dashed line in the plot). Even if the number of modules belonging to the three classes is considerably different, it strikes to observe in Figure 17 a) that 100% of Class A modules (fully transparent encapsulant) belong to Group 1, as it could also be inferred from Figure 15. Interestingly, indeed, modules belonging to Class A show extremely moderate losses in FF as well (and not only in I_{sc}), suggesting that the electrical circuit is not affected by corrosion nor increased series resistances.



It is also interesting to observe that Class A and C are clearly disjointed. While power variations for Class A are limited to the range $[-1.5\%, -8.0\%]$, those of Class C modules (with uniform yellowing and in some cases browning) vary in the range $[-58\%, -9.7\%]$ (with the exception of one module having $\Delta P_{\max} = -7.8\%$).

The clear demarcation line for the two classes reflects the remarkable reduction in I_{sc} for all modules belonging to Class C. For modules in Class C, different root causes lead to loss in performance. For a sub-set of devices, the power loss can be attributed exclusively to a reduction in current, due to encapsulant browning (power degradations between 12% and 18%). For another sub-set of modules belonging to this class, a reduction in FF is clearly superimposed to the loss in I_{sc} , indicating that these modules are affected not only by encapsulant browning but also, most likely, by problems in the interconnections or hot spots. Modules falling into this category are described in paragraph 0. In Figure 17 we show the intermediate case of Class B modules (with localized and mild yellowing). Here, the power losses are (with the exception of an outlier) limited to 26.6% (i.e. 0.76%/y). As we can see, the power losses span the full range so that Class B modules belong both to Group 1 and to the portion of Group 2 members experiencing the least degradation. In addition, the relationship between the electrical parameters is more varied for this class: in some of the devices the P_{\max} degradation is dominated by a loss in I_{sc} , while others mainly degraded because of a loss in FF. Furthermore, we note that none of the 288 modules experienced significant reductions in V_{oc} , consistently with the fact that no module showed interruption of the electrical circuit nor any sign of potential-induced degradation (PID). To summarize the relationship between the three discoloration classes and the long-term performance degradation rates after 35 years in the field, we report in Table 5 the composition of the two groups presented previously. As we can see, Group 1 (mean power degradation of only 0.20%/y) is mainly composed by modules in Classes A and B, with only a few number of modules from Class C. Group 2, instead, does not contain any module of Class A, and a high fraction of the group is given by modules of Class C (88.3% of the modules in Group 2).

		Class A (encapsulant as new)	Class B (localized mild yellowing)	Class C (uniform strong browning)
Total 288 modules	# modules	27	59	202
	Share	9.4%	20.5%	70.1%
Group 1 (mean degradation -0.20%/y) 66 modules	# modules	27	33	6
	Share	40.9%	50.0%	9.1%
Group 2 (mean degradation -0.69%/y) 222 modules	# modules	0	26	196
	Share	0.0%	11.7%	88.3%

Table 5: Composition of the two groups of modules – distinguished based on their long-term degradation rates after 35 years of field exposure (2017) – with respect to the three classes of encapsulant discoloration (Class A, B, and C). Group 2 (with the highest degradation rate) is largely made of Class C modules, and does not contain any module of Class A.

Front delamination

A vast majority of the modules are concerned by some type of front delamination (87.5% of the modules). Front delamination can consist in the separation between the glass and the front encapsulant, or between the front encapsulant and the cell. Front delamination can pose a safety risk when it forms a continuous path between the edge of the module and the electrical circuit, allowing for water ingress. An example is shown in Figure 18.

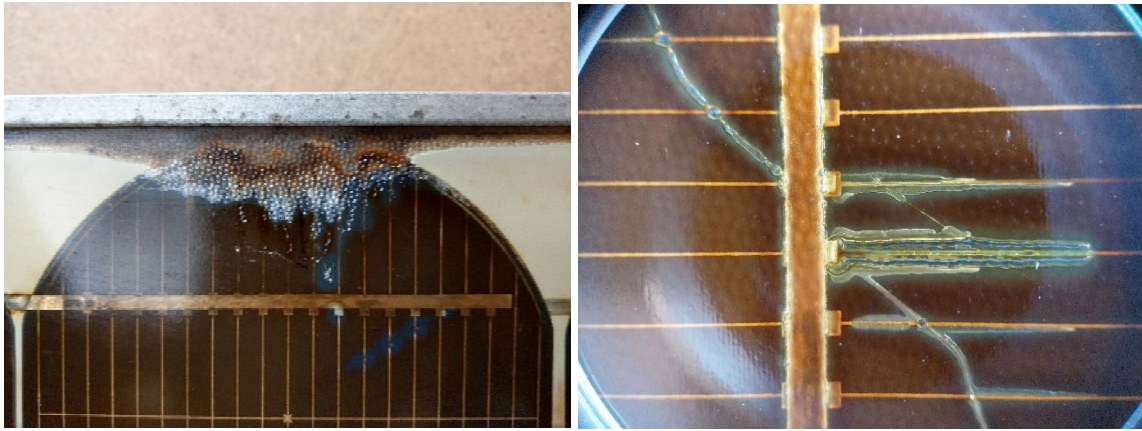


Figure 18: front delamination defect: left major, right minor.



Figure 19: front delamination minor defect: bubbles.

Modules presenting such defect and that, in addition, did not pass the insulation test (performed in 2017) are classified here as cases of major delamination. The very narrow distance between cells and frame (~5 mm) is an intrinsic weakness of this product design. On the other hand, when front delamination does not result in insulation issues we define it as a minor delamination (Figure 18), which therefore does not constitute a safety hazard per-se. Delamination may appear in the form of bubbles (Figure 18b) and, when at the cell/encapsulant interface, it commonly appears above the interconnect ribbons or the cell cracks, as shown in Figure 19. When the delaminated area is directly over a cell, optical losses cause a reduction of the cell current, which results in a dark area in the EL picture (see module in Figure 9). The part of the cell that is not affected by delamination will work at higher temperature with respect to the surrounding cells, due to a current mismatch: such local heating is clearly visible by IR imaging (see Figure 10). The actual impact of delamination (both major and minor) on module performance is in general not easy to assess, because (i) it is proportional to the size of the delaminated area, which is in general small, and (ii) most often other degradation mechanisms are acting in parallel (such as encapsulant yellowing, corrosion of fingers and ribbons, etc.).



Backsheet damage

The backsheet material employed in these Arco Solar modules is made by three layers: Tedlar®/metal/Tedlar®. The metal plate is steel, as specified in the original datasheet and further verified during our inspection by means of a magnet. The presence of a metal plate makes the backsheet impermeable to water ingress, in contrast with the majority of the modules deployed in PV installations, which use a polymer foil backsheet. The backsheet in the Arco Solar modules presented a degradation mode that is peculiar to its design: a delamination of the external Tedlar layer from the metal plate. For most modules, indeed, the external Tedlar layer either (1) presents bubbles and wrinkles (66% of the modules) or (2) is to a large extent detached from the metal plate (32%). This can be seen in Figure 20 a) and b), respectively. When visible, the steel plate generally appears rusted, but without any major signs of rupture or cracks, which would severely compromise the sealing and the insulation of the electrical circuit. After performing a destructive analysis on one of the 288 modules, however, we noticed that the metal plate was cracked – even if still covered by the external Tedlar layer – and highly corroded in proximity of a corner. Burn marks were present as well, possibly the effect of arching due to the ingress of water from the module's corner (see Figure 20 c)). A cracked metal layer seriously compromises the insulation of the module, which would not pass a wet, and possibly a dry, insulation test. In the remainder of this paper, we will treat cases in Figure 20 a) and b) as a minor BS damage (i.e. partial or complete delamination of the external Tedlar layer from the – intact – steel plate). A major BS damage is flagged, instead, for this specific BS design, when the steel plate itself is cracked or damaged (Figure 20 c)). As the full detection of cracks in the metal layer would require a destructive analysis by separating the external polymer layer in all modules, we chose not to have any statistics on this failure mode. From the results of the insulation test (see Table 6), however, we speculate that this major damage affects only a minimal part of the modules and that, in general, the backsheets after 35 years are still working properly, providing electrical insulation and preventing moisture ingress into the encapsulant.

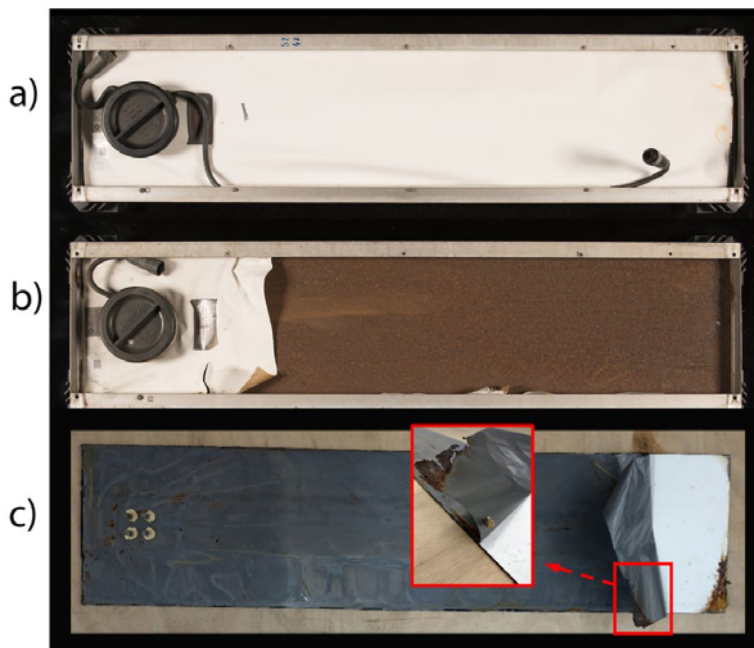


Figure 20: Damages to the modules' backsheet: a) bubbles & wrinkles in the external Tedlar layer leading to a partial delamination of this layer from the steel plate (not visible); b) Nearly complete delamination of the external Tedlar layer from the steel plate; c) corrosion and breakage of the internal steel plate, probably due to delamination and moisture ingress at the module's corner. Cases a) and b) are classified here as a minor backsheet damage, while case c) is a major backsheet damage (major safety risk).



	Ground continuity check	Diode functionality test	Insulation test		Wet leakage		Hot Spots		Junction box
Year	2017 (35 yrs)	2017 (35 yrs)	2010 * (28 yrs)	2017 ** (35 yrs)	2010 (28 yrs)	2017 (35 yrs)	2010 * (28 yrs)	2017 ** (35 yrs)	2017 (35 yrs)
Modules tested	288	288	285	276 *	285	43 ×	288	274	288
Passed	95.5%	88.2%	97.2%	91.3%	83.3%	95.3% (41 out of 43)	87.2%	71.5% (Minor / no HS)	96.9% (JB attached)
Failed	4.5%	11.8%	2.8%	8.7%	15.6%	4.6% (2 out of 43)	12.8%	28.5% (Major HS)	3.1% (loose JB)
<p>* Insulation test according to IEC 61215 [10].</p> <p>** MBJ's High Potential test (MBJ); different procedure than in IEC 61215 [13].</p> <p>* Insulation test could not be performed on the 12 modules out of function ($\Delta P = -100\%$).</p> <p>× Wet leakage on a subset of the best performing modules.</p> <p>(*) Hot spots determined by IR imaging outdoors.</p> <p>(**) Hot spots determined from combined analysis of EL, VI, and IR images.</p>									

Table 6: Summary of the results of the safety tests performed in 2010 and 2017. Data about hot spots and defects in the junction box (i.e. partial detachment from the backsheet) are also reported.

Cell cracks

The Arco Solar modules of the TISO plant consist of 35 mono-crystalline Si cells. Cells are round with a diameter of 102.5 mm and a thickness of 330 μm . Over the years, the PV market has been constantly decreasing the thickness of cells to save on manufacturing costs, with the drawback of making them more fragile and prone to fracture. The cells employed in the ARCO Solar modules are thus more resistant against cracks than today's mono-crystalline c-Si cells, whose thickness is typically in a range as low as 180 μm . Nonetheless, many modules in the TISO plant present cracks in the cells, some of them also visible by the naked eye. By performing EL imaging on all the 288 modules, we classified the cracks into two categories, partly following the definitions proposed in ref. [36]: we define as a minor crack any crack that appears as a dark line or results in cell regions with a reduced EL intensity; a major crack represents instead a region completely separated from the electrical circuit (appearing as completely dark). Examples are shown in Figure 21. With respect to the nomenclature used in [36], minor cracks include "Mode A" and "Mode B" cracks, while major cracks correspond to "Mode C" cracks. As can be seen in Figure 22, minor cracks do not have a clear impact on the power reduction after 35 years compared to modules without cracks. Major cracks seem, instead, to be correlated with an additional -5.4% power variation. The large variance is due to the fact that (i) the current (and power) loss strongly depends on the portion of the cell affected by the defect [33], and (ii) other degradation modes might be present. We point out that some modules present cracks that span over more than one cell, suggesting that they were probably induced during transport or installation. These cracks are generally of the minor type.

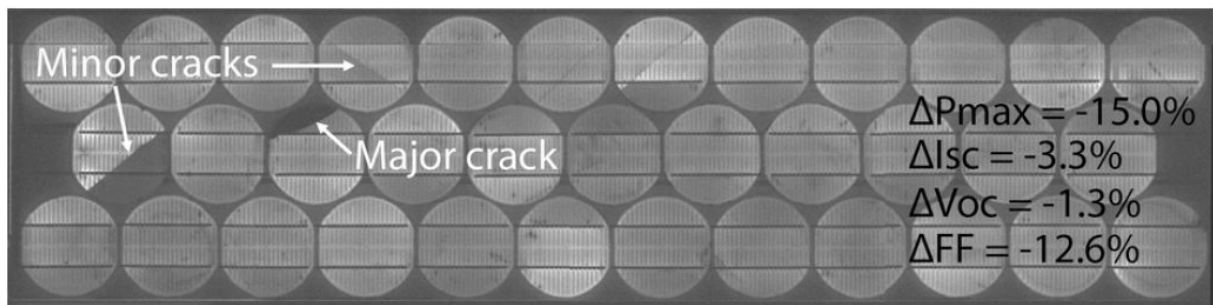


Figure 21: Examples of minor and major cell cracks as defined in this work. The values indicate the relative variation (2017 vs 1982) of the electrical parameters with respect to the initial values (average values of the reference modules).

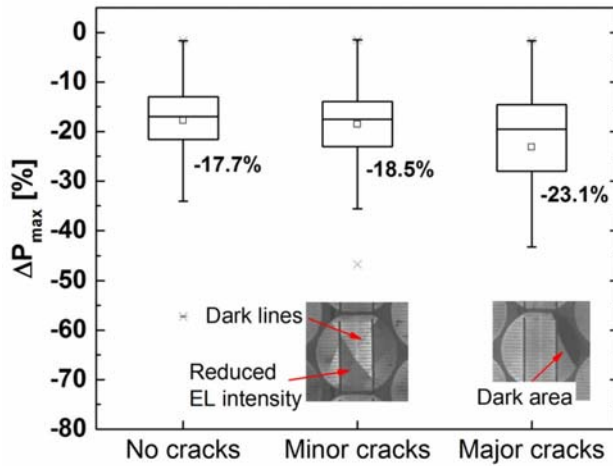


Figure 22: Box plot showing the relative power variation after 35 years for modules containing cells with major cracks, modules with only minor cracks, and modules with no cell cracks. The two regions in the boxes depict the first and third quartile, with the internal line indicating the median; the small square (and the number) denotes the mean value.

Internal circuitry corrosion

Module electrical interconnections, or internal circuitry (IC), are constituted by three levels of metallization. Following the nomenclature given in [37] and starting from the silicon surface we find: (1) the cell fingers and busbars, which are metallization lines directly printed over the silicon; (2) the ribbons, which are soldered over the cell's busbars and connect one cell to the other; (3) the string interconnects, which are metallic ribbons at the extremity of a line of cells, along the short sides of the module, not directly soldered on the cell but on the ribbons only. All these different interconnections can be subjected to degradation. In case of a strong oxidation, corrosion appears in the interconnections. Figure 23 a) shows a module with corroded interconnections on the cells above and close to the junction box. While in many cases the correlation between the IV curve and a given degradation mode is not straightforward, in this module we could identify a clear effect of interconnection corrosion on the 2017 IV curve (see Figure 23 b), characterized by an increased series resistance. The modules affected by IC corrosion are also affected by encapsulant yellowing.

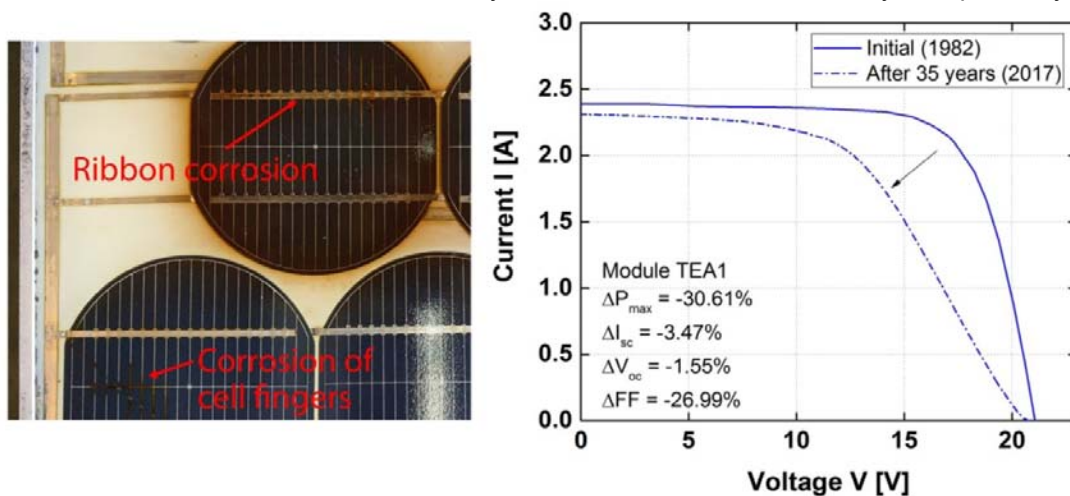


Figure 23: Left: IC corrosion on a reference module (module TEA1). This module belongs to Class B (mild and localized encapsulant yellowing). Right: IV curves of the module TEA1 as measured initially (1982) and after 35 years. The strong increase in series resistance is most likely due to the corrosion in the interconnections. This effect results in a loss in FF of -27% .



Hot spots

We define a hot spot as a cell (or an area of a cell) that is operating at temperature higher than the one of the surrounding cells. Some causes of hot spots are the presence of a cell that is forced to operate in reverse bias, for example because of a major crack, or the presence of resistive interconnections. Often, cells suffering from hot spots are those located over the junction box (see Figure 24), due in general to the worse thermal balance introduced by the box itself, and, in particular, for the unreliable electrical connection of the diode, without stress relief, often causing heating. Hot spots, in combination with a defective by-pass diode, may in the long-term seriously damage the surrounding materials and lead to burn marks (see next section).

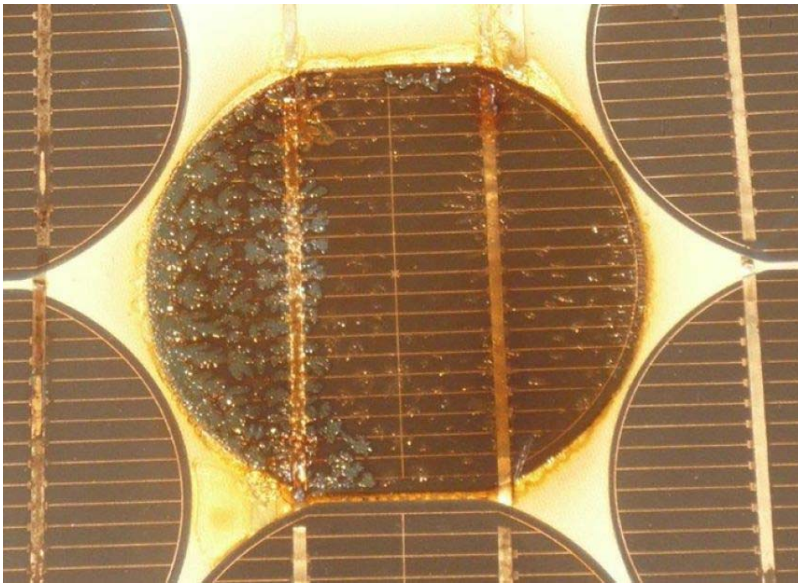


Figure 24: In this module, the cell located over the JB shows a particularly severe case of hot spot (the cell is hotter than the other cells), which also lead to burn marks diffused all over the encapsulant and on the interconnect ribbons. IC corrosion is present as well, also visible in the interconnect ribbons on the left-side cells.

Burn marks

Burn marks are the effect of burns over the cells, interconnects, encapsulant, or backsheet and are caused by excessive heat. Burn marks were identified by visual inspection. Some of them are located on the interconnect ribbons, in correspondence to heating due increased series resistance (ribbon corrosion or partial ribbon detachment from the cell busbar, i.e. solder bond failure). Others appear on the encapsulant, often in proximity of cells with localized heating (hot spot), as was shown in Figure 10. Burn marks can also appear on the backsheet (not frequently observed here), where they may cause loss of insulation, see Figure 25.



Figure 25: Burn marks in the backsheet constitute a safety risk as they may cause loss of electrical insulation. The inset is a zoom on the defective area.

Junction box

The junction box, hosting the module terminals and the by-pass diode, is closed on all sides (see Figure 26). In contrast with the designs commonly in use today, glued to the backsheet only along the four edges, in this case the contact surface with the backsheet is the full internal area of the junction box. Such weatherproof design allows the junction box to protect the electrical components from moisture, snow, or salt fog. In 9 modules (3.1% of the total) the junction box was found to be partially detached from the backsheet. By opening and inspecting some junction boxes, we found only in few cases oxidation of the metallic terminals and components (not shown here).



Figure 26: The inside of a junction box (the cover was removed for the inspection): the junction box is completely closed, also at the side in contact with the backsheet, which makes it particularly impermeable.

Potential-induced degradation

From the IV curves we do not observe shunt resistance losses and we tend to exclude that the modules suffer from potential-induced degradation (PID), see Figure 14, right). On the one hand, we would expect the low resistivity of the encapsulant, PVB, to make the modules sensitive to PID. On the other hand, the modules underwent several rearrangements in the PV plant over the years, with:

1. Four different electrical layouts (number/length of strings) and consequent system maximum voltages;
2. modules resorting (when changing the inverters) based on a current matching criterion, so that the same modules may have been exposed to negative and positive (regeneration) potentials to ground over the years;
3. 36 modules were kept exposed in open-circuit conditions for approximately 10 years.

We thus do not observe the phenomenon, but changing the operation conditions of the modules several times over the years may have influenced the occurrence of PID. The mild weather conditions in Lugano (high humidity is typical of winter time, when temperatures are low) and the relatively low string voltages might also have helped in preventing PID.



Multiple degradation modes

So far, we have addressed single degradation modes, describing them and trying to assess their impact on performance loss whenever possible. However, as mentioned, often multiple degradation modes occur simultaneously on the same module, so that correlating a given degradation mechanism to overall loss in module performance becomes a difficult task. An example is given in Figure 27, which shows a module affected by a harsh yellowing of the encapsulant (Class C) and possibly of the backsheet, delamination in proximity of the edges, leading to water ingress and burn marks between edge and cell, and severe oxidation of the contacts. The effects of the different aging mechanisms can be seen very clearly in the IV curve of the module, displayed in Figure 28. With respect to the initial 1982 IV curve, the 2017 one exhibits a reduction in I_{sc} . Encapsulant yellowing and, in a minor part, a front delamination over the cells are the main causes of this effect. The change in the shape of the curve close to the maximum-power point, typical of the presence of an inhomogeneous series resistance in a cell/ module, can be ascribed to oxidation of the interconnections and to the presence of cracks that isolate some regions of the cells. With respect to the overview of modules' electrical performance in Figure 17, this module is the one showing the most extended power degradation (i.e. -58%), characterized by a combination of I_{sc} and FF losses.

As we can see in Figure 28 on the right, the power degradation over the years is driven by FF degradation, and it follows a polynomial rather than a linear curve for a series resistance impacted module. We should however highlight that in 2001 (after almost 20 years of exposure) this module was still performing at 90% of its nominal power.

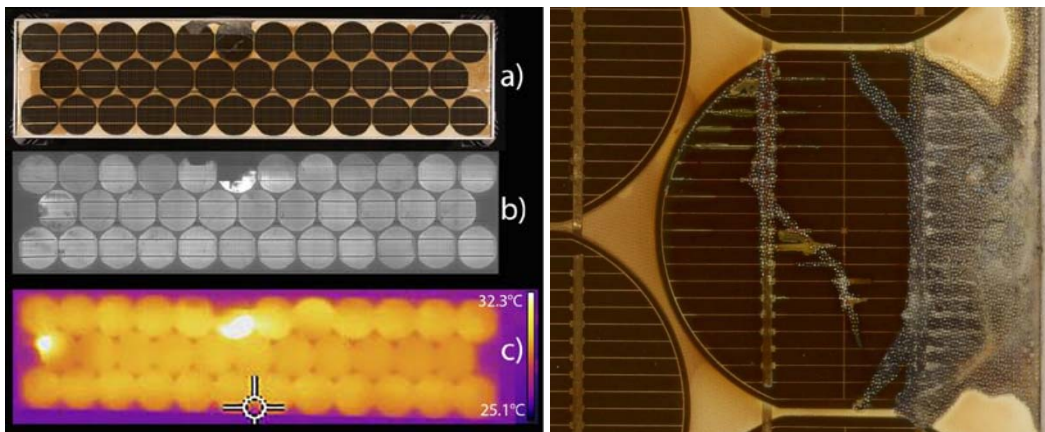


Figure 27: A severely degraded reference module (TEA9) affected by multiple degradation modes: a browning of the encapsulant affecting the three strings, front delamination, cell cracks, discoloration and corrosion of the interconnection ribbons.

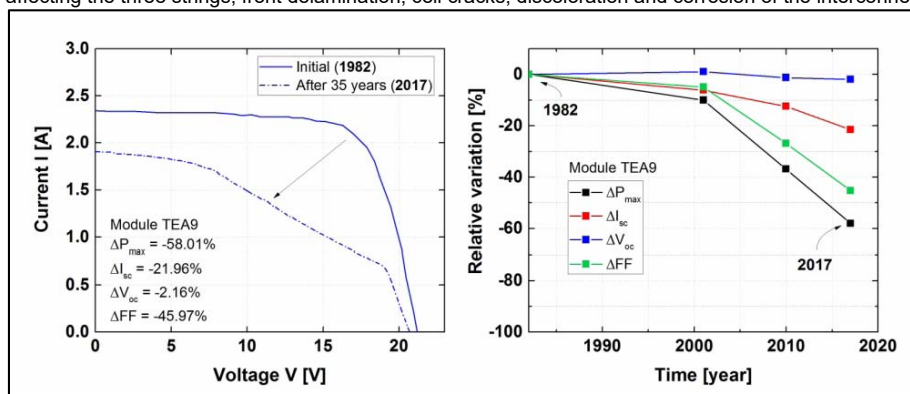


Figure 28: Comparison of the initial 1982 and 2017 IV curves for the reference module of Figure 27.



Frequency of the degradation modes

We discuss now the frequency of occurrence of each of the degradation modes described so far, as detected in 2017 (35 years). For some degradation modes we distinguished a minor and a major type: the minor type is represented in the bar plot in Figure 29 with a dashed pattern. The bars are colour coded by severity on safety. Note that, as most modules are affected by multiple degradation modes, the percentages of occurrence do not add to 100% (i.e. the plot is not a Pareto chart). We observe that the dominant degradation mode is minor backsheet damage (98% of the modules affected). Other frequent degradation modes are minor front delamination and major encapsulant discoloration (i.e. Class C modules). In the appendix of TISO publication [2] we discuss more in details the severity of each degradation mode in terms of performance loss, detection ability, and safety, by performing a failure mode and effect analysis

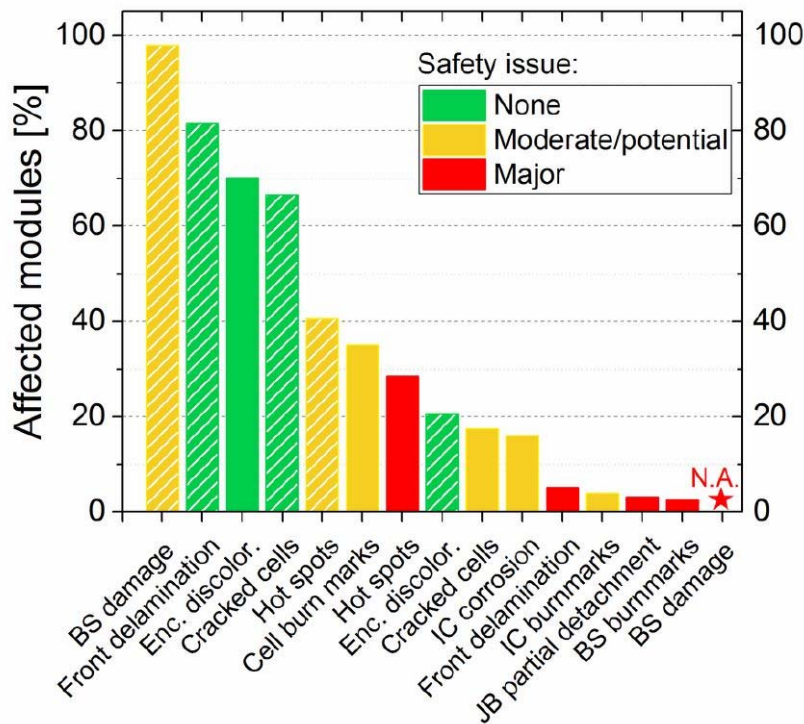


Figure 29: Comparison of the initial 1982 and 2017 IV curves for the reference module of Fig.

Safety issues

When assessing the performance of a PV plant, an essential requirement is safety in operation. The PV modules (and other components) need to operate without endangering people at work on the site. This section reports the results of the safety tests performed in 2010 and 2017. The capability of modules to provide electrical insulation was assessed by insulation and wet leakage tests. Insulation tests were performed in 2017 on all the modules, with the exception of the 12 ones (4.2% of the total) that are not operational any longer. The results indicate that for most modules the backsheet and the full module package is still assuring a good level of electrical insulation. Wet leakage (WL) tests were then performed to verify the modules insulation in wet conditions. Due to time constraints, in 2017 we restricted WL tests to a sub-set of 43 modules, chosen among those that successfully passed the



insulation test (all modules belonging to Class A and the best performing modules in Class B). Only 2 of the 43 modules failed the test (see Figure 30 below). A more complete statistic on WL performance is available for year 2010 – after 28 years of exposure – when the full set of modules was subjected to testing. The occurrence of hot spots is also reported in Table 6, even though we point out that hot spots might not be as dangerous for modules with a metal-sheet containing backsheets as for modules packaged with a conventional polymer backsheet.

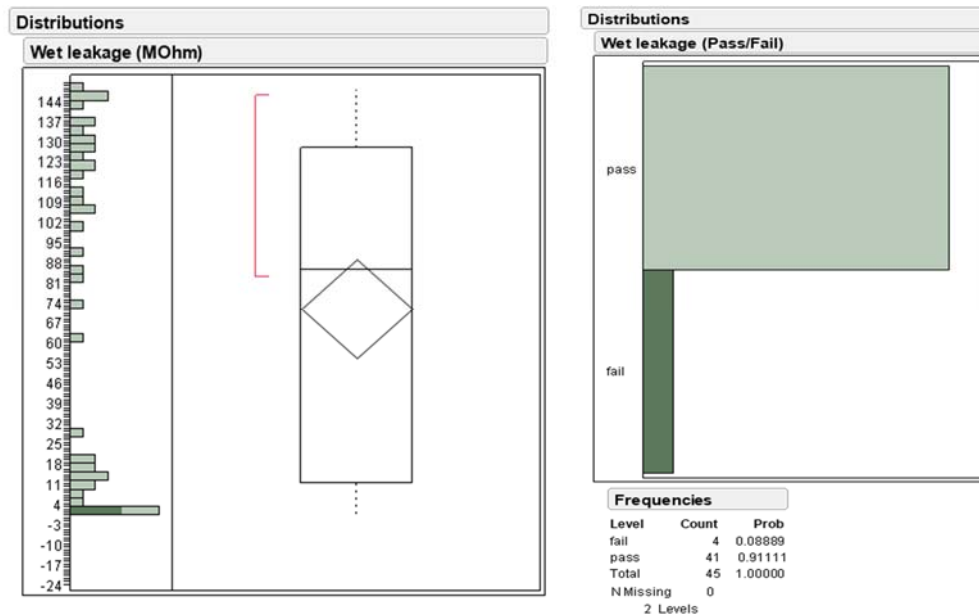


Figure 30: Results of wet leakage test: on the left the distribution of insulation resistance in MOhm is reported, on the right the Pass/Fail results according to the IEC requirements. On a total number of 43 tests (2 modules were tested twice because of interconnection problems), 2 failed.

Summary of visual inspection and safety related results

Overall, performance losses are mainly caused by encapsulant discoloration, series resistance increase and/or a combination of the two mechanisms that led to the most severe drops in P_{max} . We can summarize the situation as follows. - Approximately 23% of the modules show a very limited degradation, below the value of 12.9% identified as the separation between Group 1 and Group 2. Such devices are all the modules from Class A (encapsulant still completely transparent) as well as 56% of Class B modules (localized and mild yellowing). - Modules for which the performance is mainly affected by I_{sc} losses only, and identified by a power drop between $-20\% < \Delta P_{max} < -12.9\%$ in Figure 17 a). - Modules for which FF losses are the main causes of power degradation. Such situation is not very common and is mainly found in modules belonging to Class B (e.g. TEA1, see Figure 17 b) and Figure 23). - 39.2% of the modules are affected by both losses in I_{sc} and FF, corresponding to devices having $\Delta P_{max} < -20\%$ in Figure 17 a). These devices show the more pronounced power losses (e.g. TEA9). Correlating a single failure mode to the performance degradation was often difficult because in most cases multiple degradation modes are present in the same module, which may contribute to the same effect. Further, one lesson learnt is that a good photographic documentation of the modules is a very effective complement to field inspection, it allowing a more complete and detailed VI. An effective VI analysis may prove to be very subjective and will depend on the expertise of the operator. Furthermore, a detailed analysis is extremely time-consuming, so that an expectable trade-off between time-consumption and effectiveness should be looked after.



Conclusions and outlook

The results of the in depth analysis of the 35 years old TISO PV plant highlighted the following points:

- The degradation rate of the electrical performances of the modules, precisely measured with indoor measurements throughout the whole life of the system are far to be uniform: 2 different groups can be identified; one with a negligible degradation rate of -0.2%/year, the other with a degradation rate of -0.69%/year, much higher but still compatible with a 25 years' warranty at 80% of the original power.
- The two distinct behaviours are most probably related to the use of different suppliers for PVB encapsulants, as discovered discussing with the R&D responsible of ARCO Solar at the time of production. Indeed, the different evolution of the yellowing of the encapsulant (browned PVB, yellowing of the central cells' row, transparent PVB) verified through the visual inspection of the 288 modules, led to the classification of modules in 3 classes, which matches the information of three different PVB suppliers. Class 'A' modules are interestingly all included in the best performers' distribution.
- After 35 years there are multiple mechanisms, working together towards a faster, not linear degradation
- The loss in short circuit current is clearly correlated to the yellowing, but further degradation modes are recognizable and not easily correlated with electrical degradation of other electrical parameters. We detected:
 - o front delamination,
 - o backsheet damage,
 - o cell cracks,
 - o internal circuitry corrosion,
 - o hot spots,
 - o burn marks,
 - o defects in the junction box
- Backsheet delamination, initiated already in 2002 and affecting the main part of the modules after 35 years, does not necessarily lead to insulation and safety problems thanks to the intrinsic redundancy represented by a second Tedlar foil protected by a metal layer
- The Tedlar®/metal/Tedlar® backsheet configuration, used together with edge sealant to preserve better the PVB encapsulant from moisture penetration, is nowadays not used anymore but can be compared to a modern glass/glass solution, more frequent on the market thanks to the advent of bi-facial modules.
- The FMEA analysis, illustrated in the appendix of the second paper, ranks the defects in terms of Risk Priority Number (RPN) dictated by: severity on performance, occurrence, detectability. Safety threats are classified but not included in the RPN calculation.
- The FMEA analysis reveals that the problems for the TISO-10 plant are, in terms of RPN: the presence of delamination paths connecting the module's edge with the cells (i.e. major delamination), and major and minor hot spots. For what concerns the effect on the performance, the main issues are JB partial detachment (responsible for the 15 modules completely out of function) and IC corrosion. Safety concerns require particular attention towards: major delamination (which in nowadays module designs is prevented to occur, at least to this extent, thanks to the larger distance between cells and frame), cracks in the backsheet's metal plate, major hot spots, backsheet burn-marks, and partial detachment of the junction box."



Finally, and most importantly, what is the relevance of this study for modern systems?

For sure, the mechanisms of degradation at the end of the bathtub curve of a PV product are very complicated to be simulated artificially, but, on the other hand, the need to demonstrate a lifetime of 30 to 40 years, further to be a marketing selling point, is one of the objectives included in the PV implementation plan of the Strategic Energy Technology (SET) Plan of the European Commission. The confirmation that some materials, used 35 years ago in the production of PV modules and still on the market in other sectors, are viable to reach higher resistance to environmental factors, can trigger other research activities focused on the accelerated testing of modern recipes with new formulations of materials. Further to this, the Mean Time Before Failure project, initiated by SUPSI in partnership with ESTI JRC in 2000, whose *“Results show that, although it is not looking good from a visual aspect, the system is working in a very satisfactory manner.”* can be renewed in order to have clearer results on the End of Life behaviour and failures occurrence of a real PV system, based upon mono crystalline Silicon technology: a focus on safety issues would be particularly beneficial for the developments in the BIPV sector.

Publications [within the project]

1. “The 35th Birthday Of The TISO-10-kW Solar Plant: Lessons Learnt In Safety And Performance – Part 1” - Alessandro Virtuani, Mauro Caccivio, Eleonora Annigoni, Gabi Friesen, Domenico Chianese, Christophe Ballif. *Progress in Photovoltaics: Research and Applications.2019.*
2. “35 years of photovoltaics: Analysis of the TISO-10-kW solar plant, lessons learnt in safety and performance – Part 2” - Eleonora Annigoni, Alessandro Virtuani, Mauro Caccivio, Gabi Friesen, Domenico Chianese, Christophe Ballif. *Progress in Photovoltaics: Research and Applications. 2019.*



References

1. Friesen T, Realini A, Friesen G, et al. TISO 10 kW: 30 years of experience with a PV Plant. In: *Proc. of the 27th EU PVSEC Conference (Frankfurt, 2012)*; 2012:3125.
2. Skoczek A, Sample T, Dunlop ED, Ossenbrink HA. The results of performance measurement of field-aged crystalline silicon photovoltaic modules. In: *Progress in Photovoltaics: Research and Applications*, 17, 4, Pages; 2009:227-240.
3. Olakonu K, Belmont J, Tatapudi S, Kuitche J, TamizhMani G. Degradation and failure modes of 26-year-old 200 kW power plant in a hot-dry desert climate. In: *Conf. Proc. of the 40th IEEE Photovoltaic Specialist Conference (PVSC), Denver; 2014*.
4. Belmont J, Olakonu K, Kuitche J, TamizhMani G. Degradation rate evaluation of 26-year-old 200 kW power plant in a hot-dry desert climate. In: *Conf. Proc. of the 40th IEEE Photovoltaic Specialist Conference (PVSC), Denver; 2014*.
5. Poverini D, Field M, Dunlop E, Zaaiman W. Polycrystalline silicon PV modules performance and degradation over 20 years. *Prog Photovolt Res Appl.* 2013;21(5):1004-1015.
6. Pozza A, Sample T. Crystalline silicon PV module degradation after 20 years of field exposure studied by electrical tests, electroluminescence, and LBIC. *Prog Photovolt Res Appl.* 2016;24(3):368-378.
7. Rajput P, Tiwari GN, Sastry OS, Bora B, Sharma V. Degradation of mono-crystalline photovoltaic modules after 22 years of outdoor exposure in the composite climate of India. *Sol Energy.* 2016; 135:786-795.
8. Sánchez-Friera P, Piliouline M, Peláez J, Carretero J, Sidrach de Cardona M. Analysis of degradation mechanisms of crystalline silicon PV modules after 12 years of operation in southern Europe. *Prog Photovolt Res Appl.* 2011;19(6):658-666.
9. Han H, Dong X, Lai H, et al. Analysis of the degradation of monocrystalline silicon photovoltaic modules after long-term exposure for 18 years in a hot-humid climate in China. *IEEE J Photovoltaics.* 2018;8(3):806-812.
10. Dubey R, Chattopadhyay S, Kuthanazhi V, et al. All-India survey of photovoltaic module degradation: 2013. In: *National Centre for Photovoltaic Research and Education Indian Institute of Technology Bombay National Institute of Solar Energy; 2013*.
11. Jordan DC, Kurtz SR, VanSant K, Newmiller J. Compendium of photovoltaic degradation rates. *Prog Photovolt Res Appl.* 2016;24(7):978-989.
12. Jordan DC, Silverman TJ, Sekulic B, Kurtz SR. PV degradation curves: non-linearities and failure modes. *Prog Photovolt Res Appl.* 2017;25(7):583-591.
13. Jordan DC, Silverman TJ, Wohlgemuth JH, Kurtz SR, VanSant KT. Photovoltaic failure and degradation modes. *Prog Photovolt Res Appl.* 2017;25(4):318-326.
14. Ceppi P, Camani M. Analysis of the first year of operation of the photovoltaic utility interactive plant TISO. In: *5th EC Photovoltaic Solar Energy conference. Athens; 1983*.
15. Camani M, Ceppi P, Iacobucci D. Performances of the grid connected photovoltaic plant TISO 15. In: *6th EC Photovoltaic Energy Conference. London; 1985*.
16. Camani M, Ceppi P. Operational characteristics of the grid connected photovoltaic plant TISO 15. In: *Proceedings of MELECON '85, Mediterranean Electrotechnical Conference, Vol. IV. Madrid; 1985*.
17. Ceppi P, Camani M, Iacobucci D. Behaviour of the modules of the photovoltaic plant TISO 15. In: *7th EC Photovoltaic Solar Energy Conference. Sevilla; 1986*.
18. Camani M, Chianese D, Rezzonico S. Long term behaviour of monocrystalline and of amorphous modules in the medium size grid connected PV plant TISO. In: *11th EC Photovoltaic Solar Energy Conference. Montreaux; 1992*.
19. Realini A, Bura E, Cereghetti N, et al. Study of a 20-year old PV plant (MTBF project). In: *17th European Photovoltaic Solar Energy Conference and Exhibition. Monaco; 2001*.



20. Chianese D, Realini A, Cereghetti N, et al. Analysis of weathered c-Si PV modules. In: 3rd World Conference on Photovoltaic Energy Conversion. Osaka; 2003.
21. Realini A. Mean time before failure of photovoltaic modules final report. In: MTBF Project: Federal Office for Education and Science; 2003.
22. Kottek M, Grieser J, Beck C, Rudolf B, Rubel F. World map of the Köppen-Geiger climate classification updated. *Meteorol Z.* 2006;15(3):259-263.
23. Joint Research Centre (JRC) PV-GIS: <http://re.jrc.ec.europa.eu/pvgis/apps4/pvest.php>
24. ASI 16–2300 Solar module Data Sheet 1981.
25. Final Report of 3rd Generation Design Solar Cell Modules, Technical Report 81-7, DOE/JPL 955402–81, Sept. 1981.
26. Charlie Gay (DOE): personal communication to MC, May 2018.
27. Domenico Coiante, *La Durata dei Moduli Fotovoltaici al Silicio Cristallino*, www.aspoitalia.it, Dec. 2010.
28. De Lia F, Castello S, Abenante L. Efficiency degradation of C-silicon photovoltaic modules after 22-year continuous field exposure. In: 3th World Conference on Photovoltaic Energy Conversion, May 11–16 2003. Osaka, Japan; 2003.
29. Abenante L, De Lia F, Castello S. Long-term performance degradation of C-Si photovoltaic modules and strings. In: 25th European Photovoltaic Solar Energy Conference and Exhibition, 6–10 September 2010. Valencia, Spain; 2010.
30. International Electro-technical Commission (IEC), IEC 60891, Photovoltaic devices—Procedures for temperature and irradiance corrections to measured I-V characteristics, IEC Geneva.
31. International Electro-technical Commission (IEC), IEC-60904-Series, Photovoltaic devices—(Parts 1 to 10), IEC Geneva.
32. International Electro-technical Commission (IEC), IEC 61215:2005, Crystalline silicon terrestrial photovoltaic (PV) modules—Design qualification and type approval, IEC Geneva.
33. International Energy Agency (IEA) “Review of Failures of Photovoltaic Modules”, Report IEA-PVPS T13–01:2014, Report 2014, Annex A: Module condition checklist.
34. Müllejjans H, Zaaiman W, Galleano R. Analysis and mitigation of measurement uncertainties in the traceability chain for the calibration of photovoltaic devices. *Meas Sci Technol.* 2009;20(7):075101.
35. Virtuani A, Stepparava D, Friesen G. A simple approach to model the performance of photovoltaic solar modules in operation. *Sol Energy.* 2015;120:439-449.
36. J. Belmont, K. Olakon, J. Kuitche and G. TamizhMani, "Degradation Rate Evaluation of 26-Year-Old 200 kW Power Plant in a Hot-Dry Desert Climate," 2014.
37. D. C. Jordan, T. J. Silverman, B. Sekulic and S. R. Kurtz, "PV degradation curves: non-linearities and failure modes," *Progress in Photovoltaics: Research and Applications*, vol. 25, no. 7, pp. 583-591, 2017.



Appendix



Description of MBJ Mobile Flasher

The MBJ mobile flasher, owned by SPF Rapperswil and used for the characterisation of the whole module set of TISO plant, is capable of performing several safety and performance tests in an automated and optimised sequence. Here below a short summary of the technical specifications:



Figure 31: MBJ mobile flasher

- Power measurement with a high performance A+A+A LED solar simulator
- Long-Pulse Flasher, for high-capacity modules
- High-resolution current-voltage (I-V) characteristic with more than 1000 measurement points
- Correction of the current-voltage (I-V) characteristic according to STC IEC60891
- Weather independent measurement at an irradiance of 200-1200 watts / sqm
- Basic accuracy of power measurement better than 3% (without dedicated reference)
- Accuracy better than 2.5% when using a dedicated reference module
- Insulated, air conditioned measurement chamber (cooling and heating)
- High resolution electroluminescence inspection of up to 20 megapixels per module
- IR camera (OPTRIS based) with up to 382x288 pixels



- Bypass diode test, detection of defect diodes
- Panel connection check
- HiPot (5kV) and ground bound test (30A, all 4 frame parts)
- Combined processing and storage of all inspection results
- Test volume of up to 400 modules per day
- Mono- and polycrystalline solar modules or thin film modules
- Panel dimensions up to 1060x1990 mm (width x height)
- Use of gas driven generator for off grid use in the field



A History Of Changes

The TISO-10-kW system has undergone several changes over the years. These include orientation/tilt of the plant, electrical configuration (number of strings, modules per string, and arrays), and type of inverter used. The set of modules used in the plant has never changed over the years.

Figure 32 shows a picture of the plant in the original configuration (taken in 2002) and one following the relocation (and repowering) of year 2010. A history of the main changes is briefly summarized in Table 7.



Figure 32: original configuration of the TISO plant (2002, left) and configuration after relocation on the Aula Magna roof (2010, right).

Year	# Modules	Tilt Angle,°	# Strings/Modules Per String	# Arrays	Inverters
1982-1989	288	65	24/12	3	ABACUS 10 kW
1989-1991	288	65	24/12	1	SOLCON—Experimental
1992-2003	252	55	12/21	3	ECOPOWER
2003-2008	288	55	4/24	3	3 x Sunny Boy 2500 SMA
2009-2010	Disassembling—Characterization, relocation, and new design (18 months)				
Since 2010	288	22°	24/12	6	6 x Sunnyboy 1200 SMA
2017-2018	Disassembling and characterization				
2019?	Possibly: new installation of a subset of modules targeting 40+ years				

Table 7: chronological history of TISO layouts..